Effects of finite bandwidth on spectroscopic characteristics of normal metals

A. Knigavko and J. P. Carbotte
Department of Physics and Astronomy, McMaster University, Hamilton, Ontario, Canada L8S 4M1
(Received 30 March 2005; published 18 July 2005)

We analyze features that appear in spectroscopic characteristics of normal metals due to a finite width of the electronic band. Electronic self-energy, renormalized density of states, optical scattering rate, and optical mass enhancement parameter are computed for the cases when the electrons are coupled to either impurities or phonons. The most significant effect of impurity scattering is broadening of the electronic band. For phonon scattering, modifications arise both on the phonon and band edge energy scales. The results contrast sharply with those for an infinite band, the approximation often employed for metals with a wide conduction band.

DOI: 10.1103/PhysRevB.72.035125 PACS number(s): 71.10.−w, 78.20.Bh, 74.25.Gz, 74.20.−z

I. INTRODUCTION

One of the most powerful spectroscopic techniques in condensed matter is optical spectroscopy where measurements are done with high accuracy. The optical conductivity can be related to the characteristics of single particle excitations. Because this method probes the self-energies indirectly, a theoretical understanding and interpretation of the results is important. In this paper we discuss the effect of a finite bandwidth in simple metals and how it manifests itself in the essential characteristic quantities of optical spectroscopy. To do this we need to compute the electron self-energy which defines quasiparticle mass renormalizations and lifetimes as well as the renormalized quasiparticle density of states and bandwidth. Recently, the angular and energy resolution in angular-resolved photoemission spectroscopy (ARPES) has improved considerably and this technique has also proved itself to be another powerful tool for the study of electronic structure. It allows a direct measurement of the electron spectral density and consequently the self-energy at each point **k** in momentum space separately. Here we will compare self-energies with optical quantities to understand similarities and differences.

It is known that many properties of metals can be understood by considering only processes confined to the vicinity of the Fermi surface. This is the main justification for the standard assumption that the low energy scale is well separated and does not interfere significantly with the high energy scale set by the width of the conduction band W. If the bandwidth happens not to be very large as compared to other characteristic energies in the system (for example phonon frequencies), it is natural to expect that its effect should be observable in frequency and temperature dependent phenomena. To our knowledge, such a situation is not well documented at present, although a number of recent theoretical works suggest its importance.[1–3]

One effect of the electron-phonon interaction for finite bandwidth is the presence of characteristic features in the renormalized density of electronic states[3] in a wide frequency range, which extends far beyond phonon energies. As one expects, these features are sharp at low temperatures and smear out as temperature increases. However, at high temperatures there is a regime where phonon scattering closely resembles impurity scattering with a temperature dependent relaxation time. In the optical conductivity this manifests itself as the complete loss of a sharp Drude peak at low frequency. Such a situation has been observed previously using the Monte Carlo technique[4] by analyzing the degree of mixing of phonon modes with temperature. A related issue is bandwidth broadening. An interaction which leads naturally to a broadening of the electronic band is the interaction between electrons and static impurities. The physical origin of this phenomenon, as discussed by Mitrovic and Carbotte,[5] is a smearing of the sharp single particle levels. When band electrons interact with phonons (or other bosons) that possess their own dynamics, the broadening of the band becomes temperature dependent. The effects related to the temperature dependent band broadening were recently discussed in connection with the high temperature behavior of the dc electrical resistivity of metals, including metallic fullerenes.[6]

Mathematically, all the above effects arise due to the requirement that the self-energy equations should be solved self-consistently. Self-consistency is often a required ingredient in solving a many body physics problem. However, it was shown by Engelsberg and Schrieffer[7] that it becomes unnecessary when an infinite band approximation is adopted. Once this approximation is relaxed, one has to bring back the self-consistency. Therefore, the effects we discuss in this paper (both the features in the density of states and the band broadening) are in fact the consequence of a finite width of the electronic bands.

Another motivation for this study is the recent experimental work on temperature dependence of the optical sum and redistribution of optical spectral weight in the high-T_c oxides.[8–11] These observations are in sharp contrast with predictions made starting from an infinite band with quadratic electronic dispersion, in which case, for example, the plasma frequency is constant and does not depend on temperature nor on the interactions. Knigavko, Carbotte, and Marsiglio[12] have shown that some peculiarities of the observed temperature dependence of the optical sum can be understood as finite band effects on the interacting electrons. Here we explore other spectroscopic characteristics.

Effects of the energy dependence in the bare density of states were addressed in the literature previously. Mitrovic and Carbotte[5] and Pickett[13] discussed consequences of energy dependent features located close to the Fermi level and extending over the phonon frequency range, which is the

situation pertinent to the A15 superconductors. More recently, Freericks *et al.*[14] reported a generalization of the McMillan-Rowell inversion procedure of tunneling data in the superconducting state using as an input the full band structure from first principle calculations. Some aspects of finite bandwidth effects in the superconducting state were considered in Refs. 15 and 16. In this paper we concentrate on a particular realization of a nonconstant density of states—the finite bandwidth—and considered its effects on the spectroscopic characteristics in the normal state in great detail while neglecting the possibility of other energy dependent features in the DOS. It should be mentioned that the effects of finite bandwidth on optical conductivity at low temperatures were studied by Yoo and Choi.[17]

Below we calculate the electronic self-energy, renormalized density of states and a number of quantities, which are frequently used in the discussion of the optical conductivity, we show their dependence on temperature and on the parameters of the microscopic models used, and provide a comparison between them when possible. We base the main portion of our discussion on the model of electrons in a finite band with sharp edges interacting with (1) impurities; and (2) Einstein bosons and then consider some cases of an extended bosonic spectrum with the energy scale $\omega_{\ln}$. Our theoretical tool is the self-consistent Migdal approximation, which assumes that $\omega_{\ln} \lesssim W$ and neglects vertex corrections. Extensions of the Eliashberg equations beyond the Migdal approximation[18] are available in the literature[19–23] (see also a discussion in the review by Gunnarsson[24]), but these go beyond the scope of this study. Impurity scattering is treated in the self-consistent Born approximation.[5]

The range of parameters in the models we use for the interacting electron-phonon system has certain limitations. These constraints are appropriately understood from the bulk of knowledge in the literature about a system with the Holstein Hamiltonian, which corresponds to our case with Einstein oscillators. The phase diagram of the Holstein model has been the subject of intense theoretical studies, especially using dynamical mean field theory.[25] A number of different many particle ground states are found. It was shown that, as the parameters of the Hamiltonian are varied, the electronic Fermi liquid could be replaced by a polaronic ground state,[26] while the Fermi liquid itself can become unstable relative to a charge density wave or a superconducting state at low temperatures.[27] We would like to emphasize that in this paper we are concerned with the properties of normal metals only, albeit with a narrow band. This means, for example, that the mass enhancement parameter λ calculated for a given electron-phonon spectral function [see Eq. (59)] should not be much larger than unity, etc.

The plan of the paper is as follows. In Sec. II we give an overview of the theoretical approach used and list definitions of the most important spectroscopic quantities. Section III is devoted to the discussion of impurity scattering. Sections IV and V deal with phonon scattering in the cases of the Einstein spectrum and some more general spectra, respectively. Section IV also contains examples of alternate bare electronic bands. Section VI is the conclusion.

II. FORMALISM

A. Model for the electronic band

The bare density of states $N_0(\xi)$ is defined by the equation

$$N_0(\xi) = \frac{1}{\mathcal{N}} \sum_k \delta(\xi - \xi_k), \tag{1}$$

where $\xi_k = \varepsilon_k - \mu$ with μ the chemical potential, ε_k the electronic dispersion function, and $\mathcal{N}$ the number of unit cells. The main model for the bare density of states that we use is the one in which $N_0(\xi)$ is assumed to be constant until it drops sharply to zero at the band edges:

$$N_0(\xi) = N_0 \Theta(W/2 - |\xi|), \tag{2}$$

where W is the bare bandwidth and $\Theta(\xi)$ is the step function. The value N_0 is the parameter of the model which in principle depends on magnitude of the hopping integrals. In our flat density of states model it would have value $1/W$ so that the total number of states in the band is 1. The chemical potential is chosen to be at the center of the band, namely $\mu = 0$. This specific case of the half-filled band is not essential for the discussion of the properties we are concerned with in this paper but simplifies the numerical computations considerably. We also confine ourselves to the isotropic situation. Another model for the electronic band is discussed briefly in Sec. IV C.

The interactions modify, or renormalize, the bare density of states. The renormalized density of electronic states (or density of states for quasiparticles) is defined by

$$N(\omega) = \int_{-\infty}^{+\infty} d\xi \, N_0(\xi) A(\xi, \omega). \tag{3}$$

It reflects the effect of interaction that are contained in the electronic spectral density:

$$A(\xi, \omega) = -\operatorname{Im} G_{ret}(\xi, \omega)/\pi, \tag{4}$$

through the real axis self-energy $\Sigma(\omega + i0^+)$. The retarded Green's function $G_{ret}(\xi, \omega)$ is defined by the relation

$$[G_{ret}(\xi, \omega)]^{-1} = ([G_0(\xi, z)]^{-1} - \Sigma(z))_{z=\omega+i0^+} \tag{5}$$

with $G_0(\xi, z) = 1/(z - \xi)$ being the free electron Green's function.

In our calculations of the optical conductivity [see Eq. (14) below and the following discussion] one more characteristic of the band structure is necessary, namely the averaged square of the group velocity defined by

$$V_\xi^2 = \frac{\frac{1}{\mathcal{N}} \sum_k \left(\frac{\partial \xi_k}{\partial k_x} \right)^2 \delta(\xi - \xi_k)}{\frac{1}{\mathcal{N}} \sum_k \delta(\xi - \xi_k)}. \tag{6}$$

Because of the isotropy assumption the dispersion ξ_k can be differentiated in Eq. (6) in any direction. For V_ξ^2 we use mainly the expression derived from the quadratic dispersion of free electrons with lower band edge at $\xi = -W/2$:

$$V_\xi^2 = \frac{2\hbar^2}{mD}\left(\frac{W}{2} + \xi\right). \tag{7}$$

Here D is the number of spatial dimensions, m the free electron mass. This choice is sufficient to demonstrate the finite band effects on optical characteristics. A nearest neighbor tight binding dispersion for electrons has also been analyzed in this paper (see Sec. IV C). This choice does not affect the main conclusions based on Eq. (7) qualitatively.

B. Electron self-energy in a finite band

The most fundamental quantity for our subsequent discussion is the electronic self-energy $\Sigma(z)=\Sigma_1(z)+i\Sigma_2(z)$. The argument z can assume any complex value, but for the discussion of the spectroscopic characteristics we need to know $\Sigma(z)$ just above the real axis, i.e., with $\mathrm{Re}\, z=\omega$ and $\mathrm{Im}\, z=\delta \ll 1$. The self-energy arises due to interactions of electrons with the various types of scatterers present in the system and it is found from a self-consistent solution of the corresponding equations. In this paper elastic impurities scattering is treated in the Born approximation, while for the inelastic phonon scattering the Migdal approximation is used.

For impurity scattering it is more convenient to deal directly with the real axis equations, which read

$$\Sigma(\omega + i\delta) = \Gamma \int_{-\infty}^{+\infty} d\xi \frac{N_0(\xi)}{N_0(0)} G_{ret}(\xi,\omega). \tag{8}$$

The parameter Γ, which has the meaning of a scattering rate, specifies the strength of the interaction.

In the case of interaction with phonons we use the self-energy equations formulated in the mixed real-imaginary axis representation,[2,28] which have the following form:

$$\Sigma(z) = T\sum_{m=-\infty}^{+\infty} \lambda(z - i\omega_m)\eta(i\omega_m) + \int_0^\infty d\nu\, \alpha^2F(\nu)\{[f(\nu - z) + n(\nu)]\eta(z-\nu) + [f(\nu+z) + n(\nu)]\eta(z+\nu)\}, \tag{9}$$

$$\lambda(z) = \int_0^\infty d\nu\, \alpha^2F(\nu)\frac{2\nu}{\nu^2 - z^2}, \tag{10}$$

$$\eta(z) = \int_{-\infty}^{\infty} d\xi \frac{N_0(\xi)}{N_0(0)} \frac{1}{z - \xi - \Sigma(z)}, \tag{11}$$

where $\omega_m = 2\pi T(m - 1/2)$, $m \in Z$ are the fermionic Matsubara frequencies, $f(\nu)$ and $n(\nu)$ are Fermi and Bose distribution functions, respectively. The electron-phonon interaction is specified in terms of the electron-phonon spectral function $\alpha^2F(\omega)$ (the Eliashberg function). The variable z can assume, in principle, arbitrary complex values. These equations allow for a fast solution method on the real axis.[28] At first, the solutions for $\Sigma(z)$ are sought on the imaginary axis only, at $z = i\omega_m$ where the integral in Eq. (9) vanishes. Then, the function $\eta(i\omega_m)$ is used to set up an iterative procedure on the real axis to find $\Sigma(\omega)$ (note that henceforth we will use real axis variable, such as ω, as shorthand for $\omega + i0^+$).

Note that the renormalized density of states of Eq. (3) can be expressed in terms of the function $\eta = \eta_1 + i\eta_2$ defined in Eq. (11) as follows:

$$N(\omega) = -\eta_2(\omega)N_0(0)/\pi. \tag{12}$$

The real axis self-energy, both its real and imaginary parts, can be determined in photoemission spectroscopy (PES) experiments, including the angular-resolved vesrion of it (ARPES). The accuracy of this technique has increased dramatically in recent years and properties of both new and traditional materials have been scrutinized (see, for example Refs. 29–34).

C. Outline of the calculation of the optical conductivity

In linear response theory the longitudinal optical conductivity $\sigma(\nu) = \sigma_1(\nu) + i\sigma_2(\nu)$ is given by the formula[35]

$$\sigma(\nu) = i\Pi_{xx}(i\nu_n \to \nu + i0^+)/\nu. \tag{13}$$

For a normal metal, the response function Π is calculated as follows:

$$\Pi_{\alpha\beta}(i\nu_n) = \frac{2e^2}{\hbar^2}\frac{1}{\mathcal{N}}\sum_k T\sum_m \left[\frac{\partial\xi_k}{\partial k_\alpha}\frac{\partial\xi_k}{\partial k_\beta} G(k, i\omega_m + i\nu_n)G(k, i\omega_m) - \frac{\partial^2\xi_k}{\partial k_\alpha\, \partial k_\beta} G(k, i\omega_m)\right], \tag{14}$$

where we have neglected vertex corrections (the Migdal approximation). The first and the second terms are the paramagnetic and diamagnetic contributions, respectively. Using the spectral representation for the Green's functions

$$G(\xi, i\omega_m) = \int_{-\infty}^{+\infty} d\omega \frac{A(\xi,\omega)}{i\omega_m - \omega} \tag{15}$$

the Matsubara sums can be performed explicitly with the following result for the real (absorptive) part of the conductivity:

$$\sigma_1(\nu) = \frac{2e^2}{\hbar^2}\pi \int_{-\infty}^{+\infty} d\xi\, N_0(\xi) V_\xi^2 \int_{-\infty}^{\infty} d\omega\, A(\xi,\omega) \times A(\xi, \omega+\nu)\frac{f(\omega) - f(\omega+\nu)}{\nu}, \tag{16}$$

where V_ξ^2 was defined in Eq. (6) above. In the main portion of the paper we use V_ξ^2 given by Eq. (7). Note that the second derivative of the dispersion, which appears in Eq. (14), enters σ_2 only, not σ_1. At small temperatures the real part of the complex conductivity is very strongly peaked. In our calculations the ξ integral is performed analytically, while the ω integral is done numerically.

Since the complex conductivity satisfies the Kramers-Kronig relation, $\sigma_2(\nu)$ can be obtained as the Hilbert transform of $\sigma_1(\nu)$:

$$\sigma_2(\nu) = -\frac{1}{\pi} P \int_{-\infty}^{\infty} d\omega \frac{\sigma_1(\omega)}{\omega - \nu}, \tag{17}$$

where symbol P reminds that the principal part of the integral is to be taken.

D. Characterization of the optical response

It was suggested in the literature[36–40] that a useful way of characterizing the optical conductivity $\sigma(\omega)=\sigma_1(\omega)+i\sigma_2(\omega)$ of a metal is to express it by the extended Drude formula:

$$\sigma(\omega)=\frac{2S}{\pi}\frac{1}{\tau_{op}^{-1}(\omega)-i\omega[1+\lambda_{op}(\omega)]}, \tag{18}$$

where $\tau_{op}^{-1}(\omega)$ is the optical scattering rate, $\lambda_{op}(\omega)$ is the optical mass renormalization and the optical sum S is defined by the integral

$$S=\int_0^{+\infty}\sigma_1(\omega)d\omega. \tag{19}$$

If all the electrons in a solid are taken into account then the optical sum is a universal constant,[41] namely $S=ne^2/2m$ where e and m are charge and mass of the electron, respectively, while n is the total number of electrons per unit volume. The optical sum is often expressed as $S=\omega_p^2/8$ with $\omega_p=\sqrt{4\pi ne^2/m}$ being the plasma frequency. If one considers less general situations, for example if one would like to concentrate on a single band of finite width, S starts to depend on parameters of the electronic system.[12]

The Drude formula, which accounts for elastic impurity scattering of electrons in an infinite band, corresponds to Eq. (18) with $\tau_{op}^{-1}=$const and $\lambda_{op}=0$. When inelastic scattering mechanisms for electrons are present, due to interaction with phonons for example, Eq. (18) is still compatible with general casuality requirements but both τ_{op}^{-1} and λ_{op} should become frequency dependent.[36,37] The two functions $\tau_{op}^{-1}(\omega)$ and $-\omega\lambda_{op}(\omega)$, which are connected by the Kramers-Kronig relations, form the real and imaginary parts of the memory function.[37,42,43] As we show later in this paper, for a finite electronic band the memory function is frequency dependent even in the case of elastic impurity scattering.

When the complex optical conductivity is known, the real and imaginary parts of the memory function can be calculated as

$$\tau_{op}^{-1}(\omega)=\frac{2S}{\pi}\frac{\sigma_1(\omega)}{\sigma_1^2(\omega)+\sigma_2^2(\omega)}, \tag{20}$$

$$-\omega\lambda_{op}(\omega)=\omega-\frac{2S}{\pi}\frac{\sigma_2(\omega)}{\sigma_1^2(\omega)+\sigma_2^2(\omega)}. \tag{21}$$

Note that such a procedure requires knowledge of the optical sum S. In this paper we calculate it directly from Eq. (19). Experimentally, when $\sigma(\omega)$ is often known in a limited frequency range, some independent estimates of S (or the plasma frequency) could be used. From an analysis of the optical quantities $\tau_{op}^{-1}(\omega)$ and $-\omega\lambda_{op}(\omega)$, which are available from experiments with good accuracy,[35,38–40] one tries to extract information about the electronic self energy $\Sigma(\omega)=\Sigma_1(\omega)+i\Sigma_2(\omega)$.

Another quantity that is often used by experimentalists in the discussion of the optical response is the partial spectral weight[11] defined as

$$S_p(\omega)=\int_0^{\omega}d\nu\,\sigma_1(\nu). \tag{22}$$

This quantity is also called the effective number of carriers,[40] the name coming from the analogy with the result of the integration of $\sigma_1(\nu)$ up to $\nu=\infty$ which is proportional to the total number of charge carriers per unit volume.

E. Dimensionless units

In the discussion of numercal results below it is convenient to use dimensionless units. We set $\hbar=1$ and measure most quantities with the dimension of energy in terms of a half of the bandwidth $W/2$. These quanities include energy ξ, frequency ω or ν, self-energy Σ, impurity scattering rate Γ, and temperature T. Densities of electronic states, both bare N_0 and renormalized N, are measured in units $1/W$. In most cases we use the same letters for dimensional and dimensionless quantities, introducing new notations only for reduced temperature $t=T/(W/2)$, reduced electron-phonon coupling strength $a=[1/(W/2)]\int d\omega\,\alpha^2F(\omega)$ and reduced impurity scattering rate $\gamma=\Gamma/(W/2)$. Optical conductivity and optical spectral weight are measured in units $\pi e^2/[2Dm(W/2)]$ and $\pi e^2/[2Dm]$, respectively.

III. IMPURITY SCATTERING IN A FINITE ELECTRONIC BAND

A. Solution for the electronic self-energy

In reduced units the self-energy equation, Eq. (8) with Eq. (2) inserted, assumes the form

$$\Sigma(\omega)=\gamma\int_{-1}^{1}\frac{d\xi}{\omega-\xi-\Sigma(\omega)}. \tag{23}$$

We recall that the convention $\omega\equiv\omega+i0^+$ is implied. The integral over ξ produces logarithms and the resulting equation can be algebraically transformed to convenient expressions shown below. There are two frequency regions. For frequencies around zero both Σ_1 and Σ_2 are nonzero. This solution can be written in the form of explicit dependencies $\Sigma_1(\Sigma_2)$ and $\omega(\Sigma_2)$ that have the form

$$\Sigma_1(\Sigma_2)=\gamma\tanh^{-1}\frac{\sqrt{1+2\Sigma_2\cot(\Sigma_2/\gamma)-\Sigma_2^2}}{1+\Sigma_2\cot(\Sigma_2/\gamma)}, \tag{24}$$

$$\omega(\Sigma_2)=\Sigma_1(\Sigma_2)+\sqrt{1+2\Sigma_2\cot(\Sigma_2/\gamma)-\Sigma_2^2}. \tag{25}$$

In this case $0>\Sigma_2>-s_{2,edge}$ where $s_{2,edge}$ is the closest to zero positive root of the equation

$$1+2\Sigma_2\cot(\Sigma_2/\gamma)-\Sigma_2^2=0. \tag{26}$$

The solution given by Eqs. (24) and (25) is valid in the range of frequencies $|\omega|\leqslant\omega_{edge}$ with

$$\omega_{edge}=\sqrt{1+2\gamma}+\gamma\tanh^{-1}\frac{\sqrt{1+2\gamma}}{1+\gamma}. \tag{27}$$

At $|\omega|\geqslant\omega_{edge}$ the solution to Eq. (23) has the form

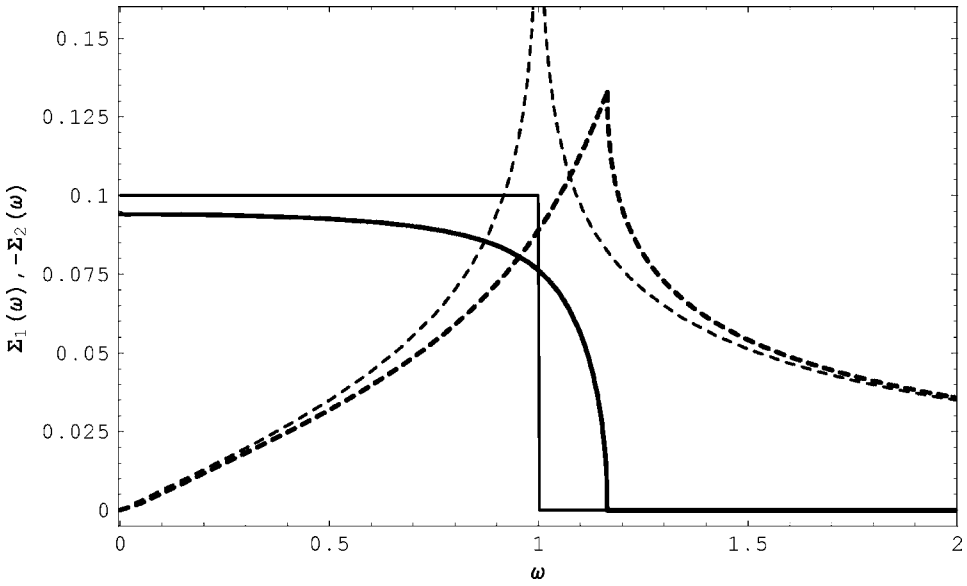

FIG. 1. Real $\Sigma_1(\omega)$ (dashed curves) and minus imaginary $-\Sigma_2(\omega)$ (solid curves) part of the electronic self-energy interacting with impurities with $\gamma=0.1/\pi \approx 0.0318$. Heavy curves correspond to a complete self-consistent self-energy, while thin curves show non-self-consistent self-energy in a finite band.

$$\Sigma_2 = 0, \tag{28}$$

$$\omega(\Sigma_1) = \Sigma_1 + \coth(\Sigma_1/(2\gamma)). \tag{29}$$

We see that ω_{edge} represents the renormalized band edge. The scattering by impurities leads to the broadening of the bare band. However, the number of states in the band does not change. For small γ (weak scattering) the renormalized band edge can be presented as an expansion:

$$\omega_{edge}(\gamma) = 1 + \gamma - \gamma \ln\frac{\gamma}{2} + \frac{1}{2}\gamma^2 + \cdots, \tag{30}$$

which is not analytic in γ.

In Fig. 1 we show results for the real, $\Sigma_1(\omega)$ (dashed), and minus the imaginary part, $-\Sigma_2(\omega)$ (solid) of the electron self-energy due to impurity scattering as a function of ω for the parameter $\gamma=0.1/\pi \approx 0.0318$. The thin curves represent non-self-consistent self-energy, namely the result of Eq. (23) with $\Sigma(\omega)$ in the integrand on the right-hand side neglected, and are for comparison with the heavy lined curves. Recall that $-\Sigma_2(\omega)$ is just $\pi\gamma$ times the density of states in the band; see Eq. (12). Therefore for the thin solid curve $-\Sigma_2(\omega)$ is equal to 0.1 up to the bare band cutoff at $\omega=1$ is reached. After that it drops discontinuously to zero. When impurities are included selfconsistently, spectral weight in the density of states (see heavy solid curve) is transferred from low energies to energies above the bare cutoff. The drop to zero in the heavy solid curve for $-\Sigma_2(\omega)$ is now gradual. The band edge is pushed from $\omega=1$ to $\omega_{edge} \simeq 1.164$ [exact value is given by Eq. (27)], demonstrating that the band broadens due to impurity scattering.

Turning to the real part of Σ we note that the logarithmic singularity in the non-self-consistent $\Sigma_1(\omega)$ (thin dashed curve) at the bare band edge is completely removed in the full self-consistent solution to Eq. (23). In this case the largest value of Σ_1 is achieved at the renormalized band edge ω_{edge}, but it is finite there, with an infinite jump in derivative. The thin and heavy solid curves eventually merge at high energies, just beyond ω_{edge}.

We emphasize that the band remains finite in the strict sense, i.e., $N(\omega)=0$ for $\omega > \omega_{edge}$, because there is no spectral weight in this frequency region. Indeed, we know that $\Sigma_2(\omega)=0$ for $|\omega| > \omega_{edge}$, therefore the spectral weight of Eq. (4) can only be of the form $A(\omega,\xi)=\delta(\omega-\xi-\Sigma_1(\omega))$. But no solution to the equation $\omega-\xi=\Sigma_1(\omega)$ is possible for any state in the bare band, namely for $|\xi| \leqslant 1$.

B. Discussion of characteristic features

In Fig. 2 we show a series of results for various values of the impurity parameter γ. From top to bottom $\pi\gamma=0.1$, 0.075, 0.05, 0.025, and 0.01 The figure has two frames and compares quasiparticle self-energies (dashed curves) with corresponding optical property (solid curves) defined in Eqs. (20) and (21). In the top frame we compare the quasiparticle scattering rate $-2\Sigma_2(\omega)$ of Eq. (23) with the optical scattering rate $1/\tau_{op}(\omega)$ of Eq. (20) and in the bottom frame we compare the real part of the self-energy $\Sigma_1(\omega)$ with $-\omega\lambda_{op}(\omega)$ of Eq. (21), the optical mass renormalization multiplied by $-\omega$. Turning first to the top frame we note that for an infinite band $-2\Sigma_2(\omega)$ and $1/\tau_{op}(\omega)$ would both be equal to $2\pi\gamma$, constant independent of ω, and extend to ∞. Two modifications are brought about by the introduction of a finite cutoff. First, $-2\Sigma_2(\omega)$ and $1/\tau_{op}(\omega)$ are no longer equal even at low energies and are both smaller than $2\pi\gamma$. The quasiparticle scattering rate (dashed curve) is above the optical scattering rate (solid curve) although the two merge as we would expect in the limit $\gamma \to 0$ (see lower curves). The second modification is the drop seen in both quantities as the band edge is approached. Remember, as we have stated before, $-2\Sigma_2(\omega)$ is proportional to the density of states of the interacting system and we see that the band edge ω_{edge} increases with increasing γ according to Eq. (27). The corresponding optical quantity is different, while its rate of decrease with increasing ω increases as we pass through ω

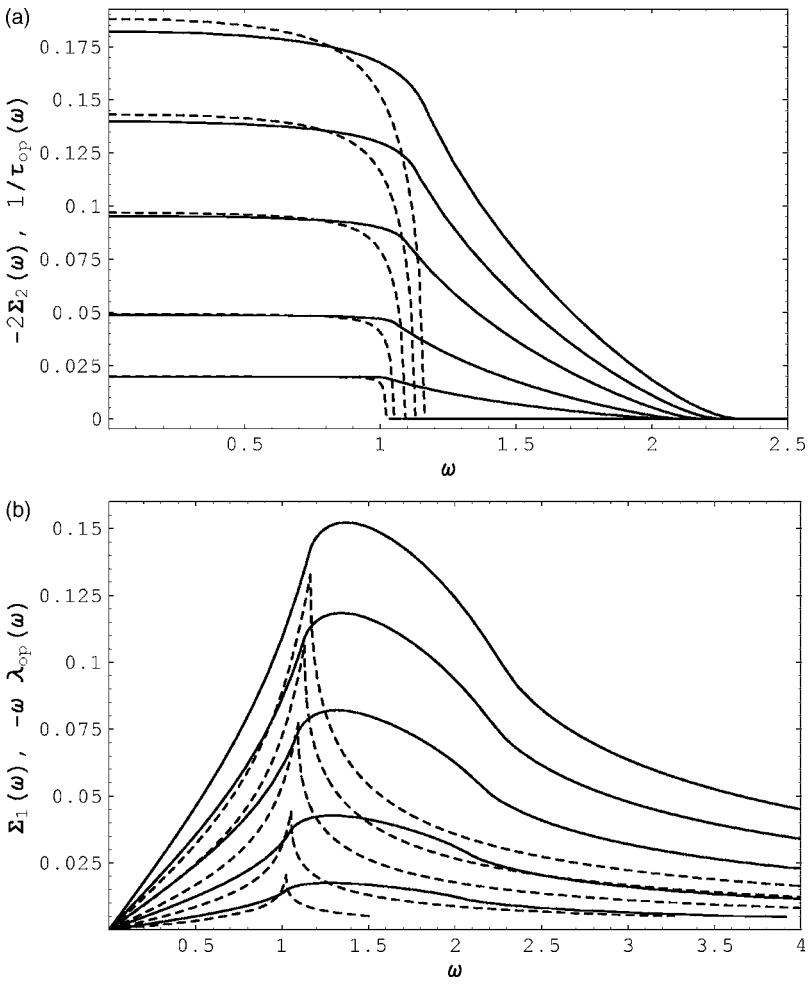

FIG. 2. (a) Comparison of quasiparticle scattering rate $-2\Sigma_2(\omega)$ (dashed) with its optical counterpart $\tau_{op}^{-1}(\omega)$ (solid) for impurity scattering with $\pi\gamma=0.1$, 0.075, 0.05, 0.025, and 0.01 from top to bottom. (b) Comparison of the real part $\Sigma_1(\omega)$ of the self-energy (dashed) with $-\omega\lambda_{op}(\omega)$ (solid) for the same values of a.

$=\omega_{edge}$, it does not go to zero. Rather it stays finite to much higher values of ω and approaches negligible values only gradually and slowly. It becomes exactly zero at $\omega=2\omega_{edge}$.

The real part of the quasiparticle self-energy $\Sigma_1(\omega)$ and corresponding optical property $-\omega\lambda_{op}(\omega)$ are compared in the lower frame of Fig. 2. In all cases the sharp peak at the band edge in $\Sigma_1(\omega)$ is clearly seen (dashed curves). As γ increases it increases in size and moves to higher energies. It is important to note that for an infinite band $\Sigma_1(\omega)$ would be exactly zero and that the curves shown are entirely due to the finite band cutoff. The solid curves for $-\omega\lambda_{op}(\omega)$ follow the same trend as we saw for $\Sigma_1(\omega)$ with two important differences. At $\omega\to 0$ the optical curve is always above the self-energy curve with both showing a linear behavior. However, the maximum in $-\omega\lambda_{op}(\omega)$ is not reached at the interacting band edge. Instead it only shows a small kink at this frequency followed by a broad maximum as compared with the dashed curve. It is not until $\omega\gtrsim 2\omega_{edge}$ that the solid curve recovers the concave upward character of the dashed curves but they remain much larger in size.

The changes in impurity self-energy brought about by a finite band edge modify the optical conductivity from its well known Drude form (infinite band) in units of $\pi ne^2/m$ with $n=1$ (half filling):

$$\sigma_1(\omega)=\frac{1}{\pi}\frac{\tau}{1+(\omega\tau)^2}, \tag{31}$$

where τ is a constant equal to $1/(2\pi\gamma)$. The profile defined by Eq. (31) for the real part of the conductivity at zero temperature (heavy solid curve) is compared with our numerical results (solid circles) in Fig. 3 for $\gamma=0.1/\pi\approx 0.0318$. The thin solid line serves as a guide to the eyes through the solid circles. The introduction of a band cutoff has increased the value of σ_1 at small ω with a corresponding decrease in optical spectral weight at higher ω where the presence of a band edge reduces the absorptive part of the conductivity and makes it zero at $\omega=2\omega_{edge}$. The increase in the dc conductivity for the parameters used here is about 6%. In the inset of Fig. 3 we show $\delta\sigma_1(\omega)\equiv\sigma_1(\omega,W=\infty)-\sigma_1(\omega,W)$, the difference between $\sigma_1(\omega)$ for infinite and finite band. This quantity starts off negative and has a crossover to positive values around, but not exactly at, the band edge ω_{edge} after which it keeps a fairly constant value. At $\omega=2\omega_{edge}$, $\sigma_1(\omega)$ ends but the Drude conductivity continues to decrease like $1/\omega^2$. It is interesting, in this regard, to compute the optical spectral weight $\delta S_p(\omega)=\int_0^\omega d\nu\,\delta\sigma_1(\nu)$ [compare with Eq. (22)] for a value of $\omega=\omega_{edge}$ and $\omega=2\omega_{edge}$. For the case considered, these are independent of frequency −0.025 and −0.01, respectively. As was made clear in the previous work

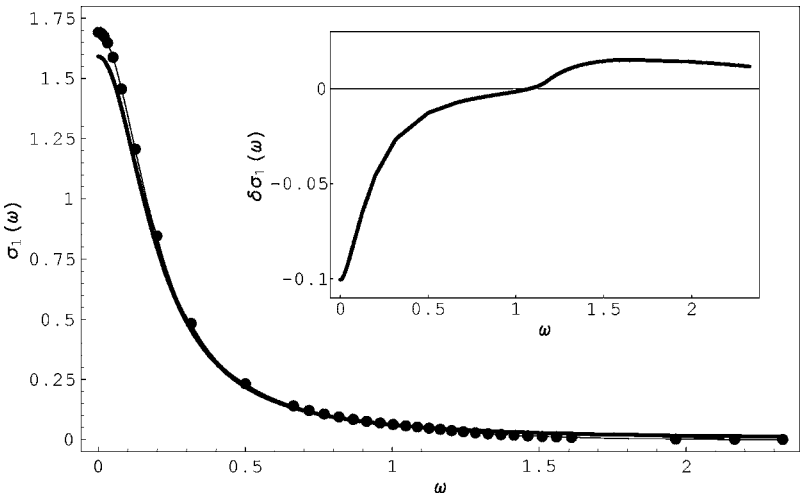

FIG. 3. The real part of the conductivity $\sigma_1(\omega)$ for impurity parameter $\gamma=0.1/\pi\approx 0.0318$ and zero temperature ($t=0$). The circles are for a finite band while the continuous curve applies to an infinite band. The inset gives the difference in optical conductivity for infinite and finite band cases as a function of ω.

of Knigavko, Carbotte, and Marsiglio,[12] the finite band cutoff reduces the total optical spectral weight below its infinite band value ($1/2$ in the units $\pi e^2/[2Dm]$). Here this difference is 2% which is small. If we had stopped at ω_{edge} instead of $2\omega_{edge}$ we would have a 5% decrease so that the difference in spectral weight between ω_{edge} and twice ω_{edge} is 3%. This is considerably smaller than for a pure Drude model which would be 5.4%.

IV. PHONON SCATTERING: EINSTEIN OSCILLATOR MODEL

A. The equations

In this subsection we model the phonons with Einstein oscillators of frequency Ω in order to gain a qualitative understanding of the band edge phenomena in the case of interaction with scatterers that have their own dynamics. Therefore we take $\alpha^2F(\nu)=a\delta(\omega-\Omega)$ where $a=\lambda\Omega/2$ with λ the mass enhancement parameter, central to the electron-phonon problem.

First, we need Eqs. (9)–(11), with the Einstein spectrum inserted, on the imaginary axis, i.e., for $z=i\omega_n$ with $\omega_n=2\pi t(n-1/2), n\in Z$ being Matsubara frequencies and t temperature in units $W/2$. They take the form

$$\Sigma_{im}(i\omega_n)=8a\Omega t\omega_n\sum_{m=1}^{+\infty}\frac{\omega_m\eta_{im}(i\omega_m)}{(\Omega^2+\omega_n^2+\omega_m^2)^2-(2\omega_n\omega_m)^2}, \tag{32}$$

$$\eta_{im}(i\omega_n)=2\tan^{-1}\frac{1}{\Sigma_{im}(i\omega_n)-\omega_n}. \tag{33}$$

Note that both $\Sigma_{im}(i\omega_n)$ and $\eta_{im}(i\omega_m)$ are pure imaginary in the case of half-filling that we consider in this paper. We used the symmetries of the function $\Sigma(i\omega_n)$ to reduce the range of summation over m.

Next, we set $z=\omega$ in Eqs. (9)–(11) and obtain the real axis part of the mixed axis representation of the finite band Eliashberg equations:

$$\Sigma_1(\omega)=8a\Omega t\omega\sum_{m=1}^{+\infty}\frac{\omega_m\eta_{im}(i\omega_m)}{(\Omega^2+\omega_m^2-\omega^2)^2+(2\omega\omega_m)^2}+a\{\eta_1(\omega-\Omega)[n(\Omega)+f(\Omega-\omega)]+\eta_1(\omega+\Omega)[n(\Omega)+f(\Omega+\omega)]\}, \tag{34}$$

$$\Sigma_2(\omega)=a\{\eta_2(\omega-\Omega)[n(\Omega)+f(\Omega-\omega)]+\eta_2(\omega+\Omega)[n(\Omega)+f(\Omega+\omega)]\}, \tag{35}$$

$$\eta_1(\omega)=\frac{1}{2}\ln\frac{[\omega-\Sigma_1(\omega)+1]^2+[\Sigma_2(\omega)]^2}{[\omega-\Sigma_1(\omega)-1]^2+[\Sigma_2(\omega)]^2}, \tag{36}$$

$$\eta_2(\omega)=\tan^{-1}\frac{\omega-\Sigma_1(\omega)+1}{-\Sigma_2(\omega)}-\tan^{-1}\frac{\omega-\Sigma_1(\omega)-1}{-\Sigma_2(\omega)}. \tag{37}$$

We solve the system of Eqs. (32)–(37) numerically, and the results are discussed in the next subsection.

It is interesting to consider the behavior of the renormalized DOS at large ω. Remember that for interactions with impurities, the renormalized band edge was sharp with $N(\omega)=0$ for $\omega>\omega_{edge}$ [see Fig. 1, where $-\Sigma_2(\omega)$ is proportional to $N(\omega)$]. In the present case of interaction with Einstein phonons $N(\omega)$ decays exponentially as $\omega\to\infty$.

For a proof we first accept this behavior as an assumption and then verify it from solution of a differential equation in the asymptotic region $\omega\gg 1$. First, we transform Eq. (34) from the mixed axis form to the real axis form which reads

$$\Sigma_1(\omega)=a\int_{-\infty}^{\infty}d\omega' P\left[\frac{n(\Omega)+f(-\omega')}{\omega-\Omega-\omega'}+\frac{n(\Omega)+f(\omega')}{\omega+\Omega-\omega'}\right]\times\left[-\frac{1}{\pi}\eta_2(\omega')\right], \tag{38}$$

This equation is convenient to obtain the asymptotic form of the real part of the self-energy:

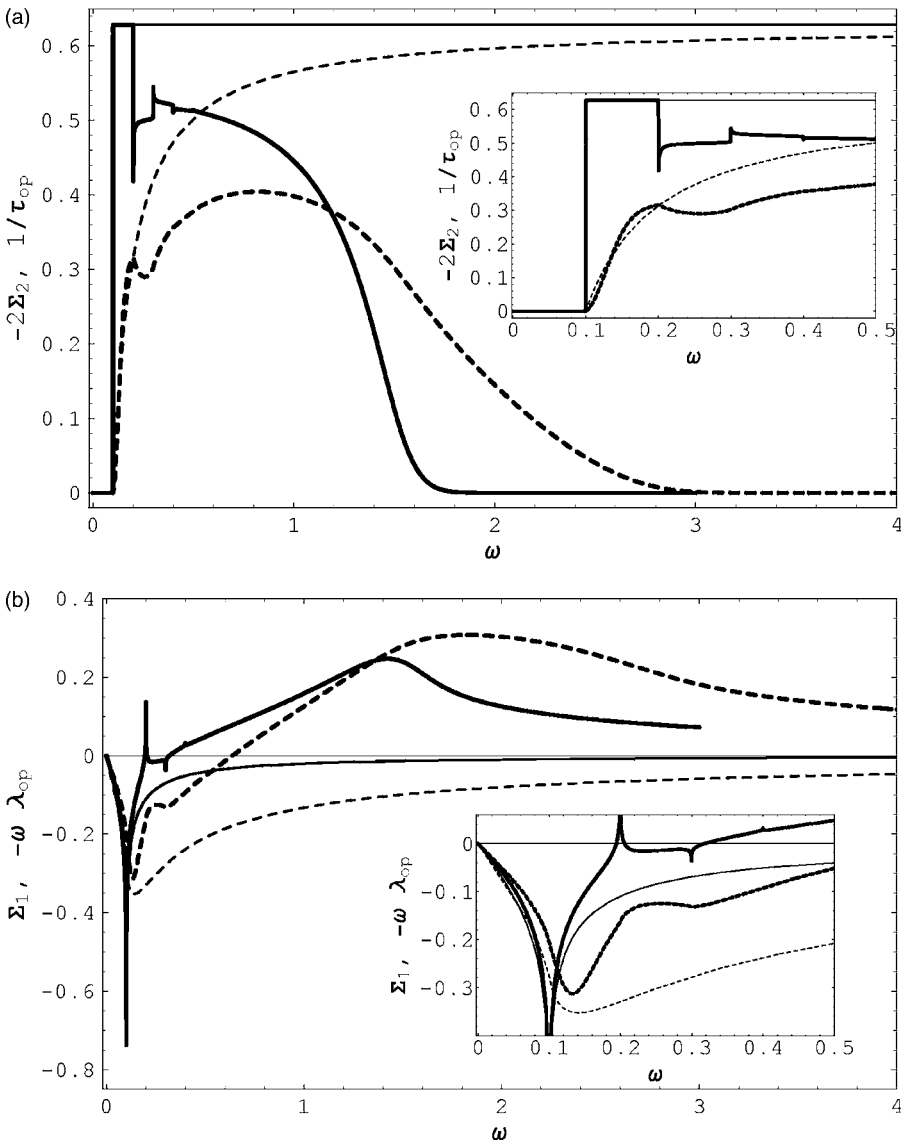

FIG. 4. Comparison of quasiparticle self-energy (solid) and corresponding memory function (dashed) for an Einstein spectrum with $a=0.1$ and $\Omega=0.1$ ($\lambda=2$). Heavy lines are for finite band while thin lines are for infinite band at zero temperature. (a) $-2\Sigma_2(\omega)$ and $\tau_{op}^{-1}(\omega)$; (b) $\Sigma_1(\omega)$ and $-\omega\lambda_{op}(\omega)$. Insets are a blowup of the low ω region.

$$\Sigma_1(\omega) \sim 2a(2n(\Omega)+1)/\omega. \tag{39}$$

Next, algebraically manipulating Eqs. (36) and (37) we obtain the following relation

$$\tan\,\eta_2(\omega) = -\frac{2\Sigma_2(\omega)}{1-[\omega-\Sigma_1(\omega)]^2-\Sigma_2^2(\omega)}. \tag{40}$$

On the left-hand side of this equation we substitute $\tan\,\eta_2(\omega) \approx \eta_2(\omega)$, and on the right-hand side Eq. (39) indicates that the ω dominates for high frequencies. Therefore,

$$\Sigma_2(\omega) \approx \frac{1}{2}\omega^2\eta_2(\omega). \tag{41}$$

Finally, the necessary differential equation is obtained by expanding Eq. (35) for $\omega \gg \Omega, 1$ and substituting Eq. (41) for $\Sigma_2(\omega)$ on the left-hand side. We arrive at

$$2a\Omega\frac{d\eta_2}{d\omega} \approx -\omega^2\eta_2, \tag{42}$$

which has the solution

$$\frac{N(\omega)}{N_0} = -\frac{\eta_2(\omega)}{\pi} \approx \text{const}\exp\left[\frac{-\omega^3}{6a\Omega}\right]. \tag{43}$$

The fact that interaction with bosons formally extends a finite electronic band to infinity can be understood as a quantum effect where virtual bosons can be excited even at zero temperature. Such a phenomenon is not present for interaction with impurities that lack any dynamics.

B. Discussion of characteristic features

In Fig. 4 we show results for coupling to a single Einstein mode and compare infinite and finite band cases. The electron-phonon interaction parameter used is $a=0.1$ and the frequency of the Einstein oscillator $\Omega=0.1$. The reduced temperature is $t=0.0001$ which is indistinguishable from zero for any practical purposes, for the finite band calculations, while $t=0$ for the infinite band. Solid curves are used for self-energies while dashed curves represent memory functions. In the main frames of Fig. 4(a) (imaginary parts) and Fig. 4(b) (real parts) we demonstrate the overall behavior

of all the quantities under consideration with frequency range extending well beyond the band edge (four times the bare width). Complimentary to this, the insets present a magnification of the low frequency region $\omega \in [0,0.5]$ which is the region of most interest in infrared spectroscopy.

Thin curves correspond to the infinite band. Analytic expressions are available in this case[35,44] and are given by

$$\Sigma_1(\omega) = a \log\left|\frac{\omega-\Omega}{\omega+\Omega}\right|, \tag{44}$$

$$\Sigma_2(\omega) = -\pi a \Theta(|\omega|-\Omega), \tag{45}$$

$$-\omega\lambda_{op}(\omega) = 2a\left(\log\left|\frac{\omega-\Omega}{\omega+\Omega}\right| - \frac{\Omega}{\omega}\log\left|1-\frac{\omega^2}{\Omega^2}\right|\right), \tag{46}$$

$$\tau_{op}^{-1}(\omega) = 2\pi a\left(1-\frac{\Omega}{\omega}\right)\Theta(|\omega|-\Omega). \tag{47}$$

The thin solid line in Fig. 4(a) is $-2\Sigma_2(\omega)$ given by Eq. (45) and in Fig. 4(b) is $\Sigma_1(\omega)$ of Eq. (44). Similarly, the thin dashed line in Fig. 4(a) gives $1/\tau_{op}(\omega)$ of Eq. (47) and in Fig. 4(b) gives $-\omega\lambda_{op}(\omega)$ of Eq. (46). The heavy solid line of Fig. 4(a) for $-2\Sigma_2(\omega)$ in a finite band shows that profound deviations from the thin solid curve start to occur above $\omega \gtrsim 0.2$ (twice the Einstein frequency), where it drops sharply only to recover slightly at $\omega=0.3$. This is a multiphonon effect completely absent in the thin solid curve (see also Ref. 3). Over the larger frequency range a renormalized band edge appears around $\omega \simeq 1.5$ and is somewhat smeared. Interaction with phonons has increased the width of the interacting band as compared to its noninteracting counterpart. In direct analogy to what was the case for impurity scattering, $1/\tau_{op}(\omega)$ (heavy dashed curve) remains large over a larger frequency range than does the quasiparticle scattering rate, extending beyond $\omega \simeq 3$. Also its drop towards zero is less abrupt.

We stress that $1/\tau_{op}(\omega)$ (heavy dashed curve) also shows sharp structures in the region which corresponds to that seen in the heavy solid curve for the self-energy although they are not as pronounced. Mathematically, this arises because the optical conductivity involves an integration over the self-energy. The prominent phonon structure just described is absent in the infinite band approximation. The thin solid curve for $-2\Sigma_2(\omega)$, which rises discontinuously at $\omega=\Omega$, is completely flat beyond this frequency while the thin dashed curve for $1/\tau_{op}(\omega)$ rises from zero at $\omega=\Omega$ gradually and smoothly towards its saturated value at $\omega \to \infty$.

Considering next the lower frequency region shown in the inset of Fig. 4(a) (up to $\omega=0.5$ only) we see more clearly the modifications that a finite bandwidth introduces into optical quantities in the infrared region. Besides the drop in the imaginary part of the self-energy at $\omega=0.2$ (twice the Einstein frequency) and the structure at $\omega=0.3$ we see that even at $\omega=0.5$ the quasiparticle scattering rate still remains depressed, by approximately 20% as compared with the infinite band case (thin solid curve). This depression in quasiparticle scattering is reflected in the optical scattering rate, when compared with the thin dashed curve. Note the shallow minimum in the heavy dashed curve in the region between $\omega=0.2$ and $\omega=0.3$. This is directly related to the corresponding multiple phonon structures in the imaginary part of the self-energy which is, as we have already said, sharper than in the optical case.

Figure 4(b) is similar to Fig. 4(a) but now it is the real part of the self-energy $\Sigma_1(\omega)$ which is compared with $-\omega\lambda_{op}(\omega)$. At zero temperature the well known logarithmic singularity at $\omega=\Omega$ for the infinite band self-energy[35] (see thin solid curve) remains a feature of the finite band self-energy as well[3] (see heavy solid curve). The thin dashed curve for $-\omega\lambda_{op}(\omega)$ shows only a weaker singularity in slope (at $\omega=\Omega$) which is followed by a broad peak centered at $\sqrt{2}\Omega$, as discussed in Ref. 44. For an infinite band both optical and self-energy renormalizations remain negative and smoothly drop to zero as $\omega \to \infty$ with the former much larger than the latter. By contrast, for a finite band, there are additional multiphonon structures and, perhaps more significantly, both quantities go through zero and become positive and large as ω increases. This qualitative difference has important implications for quasiparticle renormalization effects in finite bands, both from ARPES[29,45–47] and optical conductivity measurements, as well as for the comparison between the two, as done recently by Hwang *et al.*[48] and by Schachinger *et al.*[49] For example, as noted by Cappelluti and Pietronero,[2] the slope of the renormalized dispersion can become considerably steeper than its bare band value at large energy, while for an infinite band the two should be seen to merge. Turning to the inset in Fig. 4(b), which shows an expanded version of the small ω region, note that the self-energy $\Sigma_1(\omega)$ (heavy solid line) drops towards zero after reaching its peak at $\omega=\Omega$ much more sharply than does $-\omega\lambda_{op}(\omega)$ (heavy dashed line). This qualitative behavior is seen in the data presented in Fig. 2 of Ref. 48 where a comparison between optical and ARPES measurements is presented. A significant test of the theory presented here would be to see the predicted region of positive renormalizations at high ω in both self-energy and memory function.

In Fig. 5(a) we compare the real part of the optical conductivity obtained for the model of Fig. 4 with its infinite band value. Since we have not included impurity scattering there is a coherent quasiparticle delta function contribution at $\omega=0$ in both cases (shown as the vertical line at $\omega=0$ in the figure). The optical spectral weight in this contribution is about 10% bigger in the finite band case, so that, just as we found for the impurity case, the dc conductivity is increased as is the optical spectral weight at small ω. Besides the delta function contribution, we see beyond the phonon energy $\omega=\Omega$, the incoherent boson assisted Holstein processes. The thin curve applies to an infinite and the heavy to a finite band. Once again we see, in this region of frequency, a buildup of optical spectral weight at the smaller ω and a drop for $\omega \gtrsim 1.4$ where the heavy curve decays much more substantially than does the thin curve. We can get additional insight into the question of spectral weight redistribution, brought about by finite band effects, from consideration of the partial spectral weight given by Eq. (22). Results are shown in Fig. 5(b). The temperature $t=0$ and the phonon parameters are $a=0.1$ and $\Omega=0.1$, as before. The thin solid

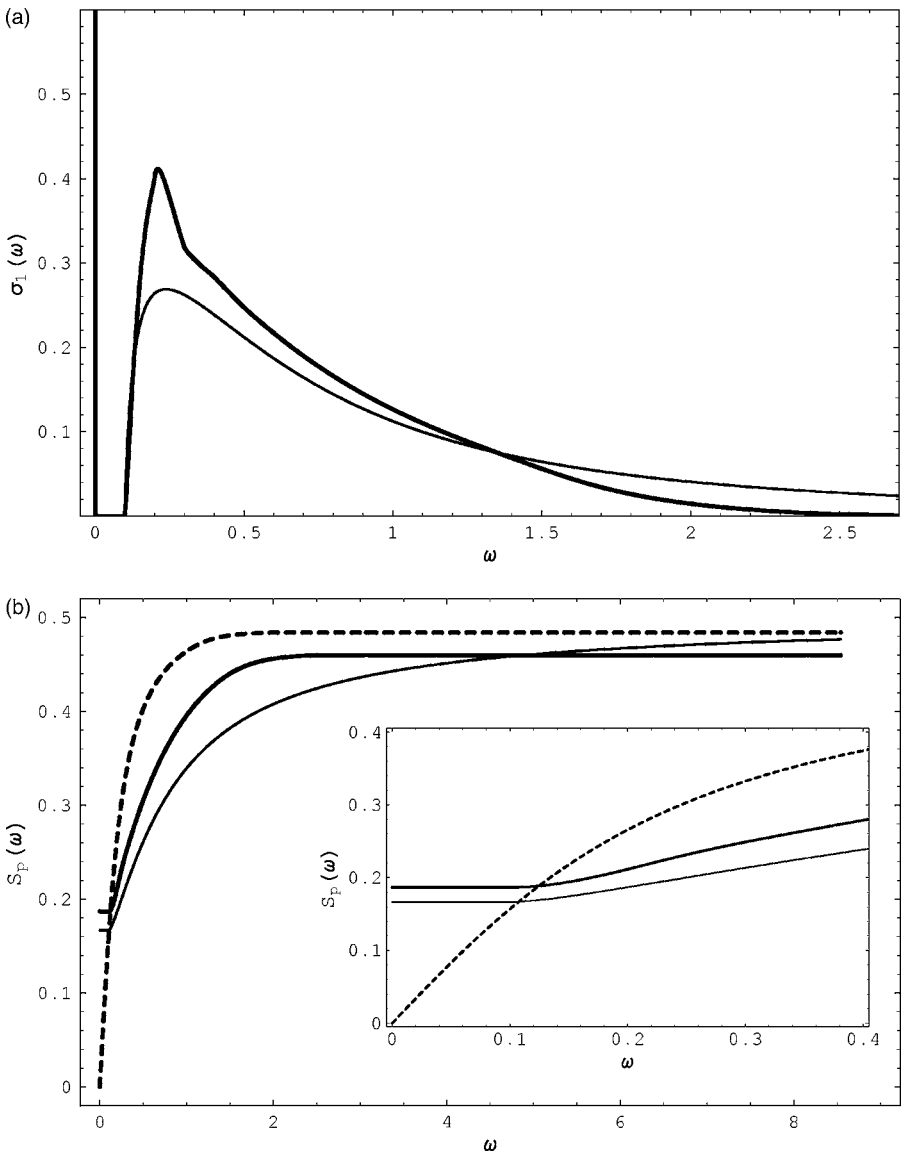

FIG. 5. (a) The real part of the optical conductivity $\sigma_1(\omega)$ for an Einstein spectrum with $a=0.1$ and $\Omega=0.1$ ($\lambda=2$) at zero temperature. Heavy curve is for finite band while thin curve is for infinite band. Both have a delta function contribution at $\omega=0$. (b) The partial optical spectral weight $S_p(\omega)$ of Eq. (22) for conductivities of frame (a) for finite (heavy solid) and infinite (thin solid) band. The values at $\omega=0$ correspond to the weight of delta function in frame (a). An equivalent impurity model (heavy dashed curve) for finite band is shown for comparison. Inset: blowup of the low ω region.

curve applies to an infinite bandwidth: $S_p(\omega)$ remains constant at a value of 0.163 until $\omega=\Omega$ (only the delta function contribution) and then begins to rise as the incoherent background starts contributing. The heavy solid curve starts at a higher value of 0.185 and increases beyond $\omega=\Omega$ faster than the thin curve. They cross around $\omega\approx 4.8$ at which point the solid curve has pretty well saturated to its asymptotic $\omega\rightarrow\infty$ limit which is 0.460. By contrast, the thin solid curve is still increasing and will reach 0.5 asymptotically at $\omega\rightarrow\infty$. The heavy dashed curve is for comparison with the previous two and is obtained for impurity scattering with $a_{imp}=0.032$. It starts at zero when $\omega=0$ but then rises very rapidly to become higher than either of the phonon curves. The saturation value at high frequencies for this curve is 0.484. The inset in Fig. 5(b) gives an expanded plot of the small ω behavior which shows more clearly the flat region below $\omega=\Omega$ for both solid curves and the rapid rise of the dashed curve in contrast.

Next we consider temperature variation of various spectroscopic quantities. In Fig. 6 we show the self-energy $\Sigma(\omega)$, that is, minus the imaginary part in frame (a) and the real part in frame (b), over a wide frequency range extending beyond the renormalized band edge for $a=0.1$ and $\Omega=0.1$. Different curves correspond to different temperatures from the following list: $t=0.0001, 0.00025, 0.0005, 0.00075, 0.001, 0.0025, 0.005, 0.0075, 0.01, 0.02, 0.03, 0.05, 0.1$. As one would expect, sharper curves correspond to lower temperatures. At the lowest temperature used, $t=0.0001$, the results are indistinguishable from zero temperature results on the scale of the figure. In this case there is a logarithmic singularity in $\Sigma_1(\omega)$ at $\omega=\Omega$ while $\Sigma_2(\omega)=0$ for $0<\omega<\Omega$. As the temperature gradually rises the sharp features in the curves corresponding to both $\Sigma_1(\omega)$ and $\Sigma_2(\omega)$ become smeared. Consider the low frequency part of $\Sigma_2(\omega)$ in the whole temperature range available. Even though there is a smearing, the characteristic gap in $-\Sigma_2(\omega)$ stays effectively intact until some crossover temperature t_{cros}, after which it starts to fill in. Simultaneously with the filling of the low temperature gap at $t>t_{cros}$ there appear changes at high frequencies, which correspond to the broadening of the renormalized band and increase of the band edge.

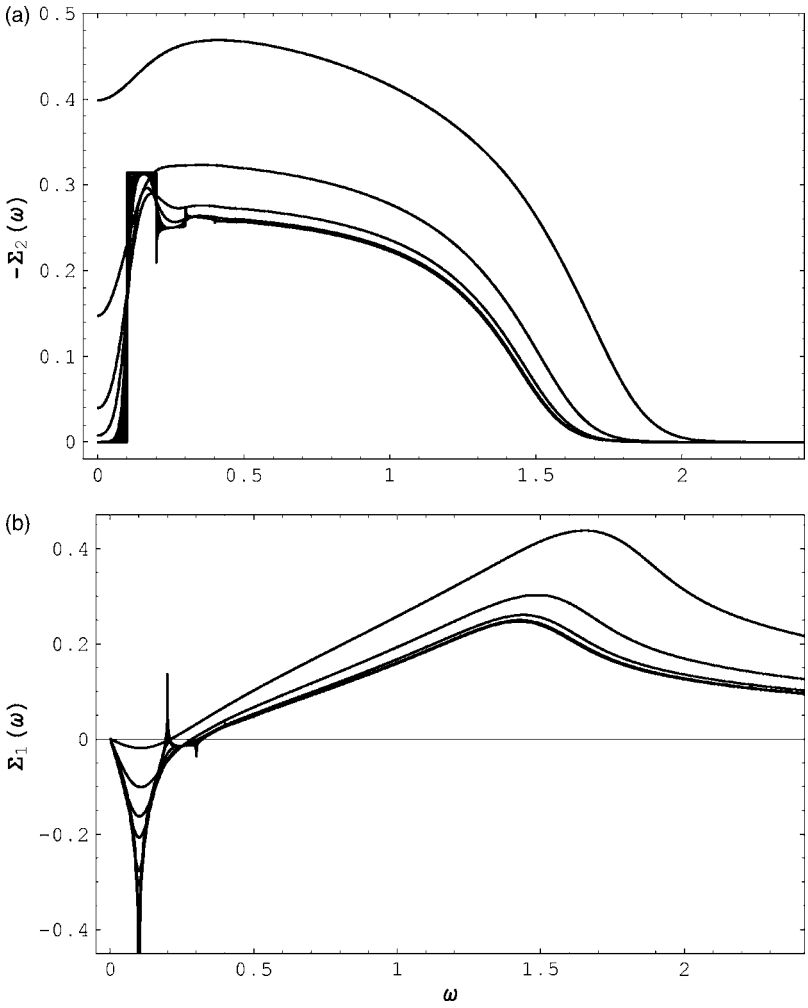

FIG. 6. Evolution of the self-energy vs frequency dependence with temperature for the Einstein spectrum with $a=0.1$ and $\Omega=0.1$ ($\lambda=2$). Frame (a) is for the minus imaginary part, $-\Sigma_2(\omega)$, while frame (b) is for the real part, $\Sigma_1(\omega)$. In each frame different curves correspond to $t=0.1, 0.05, 0.03, 0.02, 0.01, 0.0075, 0.005, 0.0025, 0.001, 0.00075, 0.0005, 0.00025, 0.0001$ from top to bottom at $\omega=0.09$ in frame (a) and at $\omega=0.9$ in frame (b).

These changes are also clearly visible in $\Sigma_1(\omega)$ of Fig. 6(b). The real part of the self-energy starts to lose its negative region at low ω and begins to look very much like the impurity case. This is physically reasonable since at high temperature fluctuations off equilibrium positions of the atoms due to temperature become larger and larger. These real displacements of the atoms appear to scatter electrons much like a static, temperature dependent impurity distribution. In fact, as shown in Ref. 4, at sufficiently high temperatures it may be difficult to classify atomic displacements in terms of phonons with well defined quasi-wave-vector quantum numbers. It should be noted that in the theoretical formalism of this paper it is implicitly assumed that, similarly to the Holstein Hamiltonian, the electron-phonon coupling is linear in atomic displacements.

The numerical value of the crossover temperature is estimated from Fig. 6 as $t_{cros} \approx 0.01$, or

$$t_{cros} \approx 0.1\Omega. \tag{48}$$

This is much smaller than the Einstein frequency Ω, meaning that t_{cros} lies well within the temperature range of applicability of our theory. As discussed by Allen,[19] quadratic and higher order terms in atomic displacements can become important as the temperature rises. In addition, the phonon will become anharmonic so that the sharp phonon modes will shift in frequency and broaden. These are all effects that go beyond the scope of this work.

What happens at $t > t_{cros}$ can perhaps be understood better if we study the renormalized (quasiparticle) density of states $N(\omega)$ of Eq. (3). It is shown in Fig. 7(a) for the same temperatures used for Fig. 6. We see that band broadening corresponds to a redistribution of the quasiparticle density of states, as the total number of states in the band stays constant, independent of temperature. A characteristic feature of energy dependence of $N(\omega)$ is the low energy ($\omega \lesssim \Omega = 0.1$) elevated "plateau" structure where the density of states is noticeably enhanced as compared to its value in the higher energy relatively flat region. After this there is a faster drop to the band edge. The plateau is followed by more structures centered at multiples of Ω. All these multiphonon structures are sharp at low temperatures and as t increases they gradually smear out, but the low frequency plateau structure remains very much distinguishable all the way to t_{cros}. After this temperature the electronic states in the plateau move gradually to the top of the band and at $t > t_{cros}$ the value of $N(0)$ decreases while the band width increases.

Note that in Fig. 7(a), corresponding to $\Omega=0.1$, the "flat" region, say $0.35 \lesssim \omega \lesssim 0.9$, can only be defined approximately. Such a region becomes much more pronounced for lower Ω (see Fig. 14 below and the corresponding discussion). On the other hand, at higher Ω such a drastic renor-

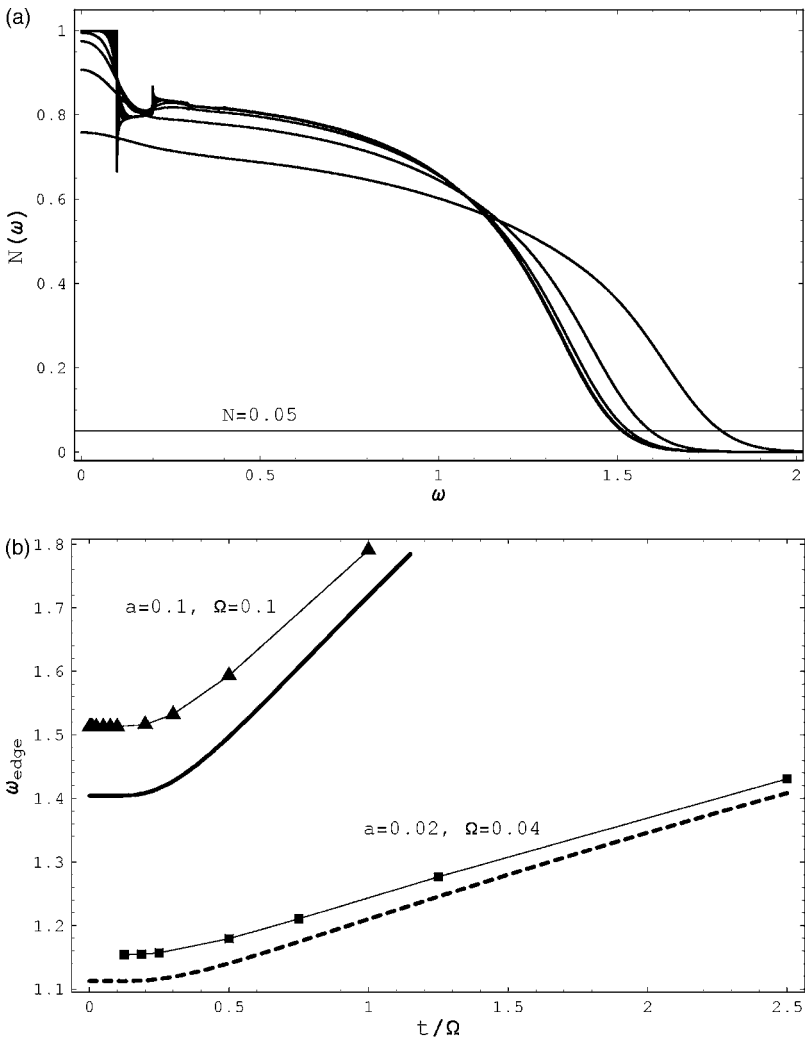

FIG. 7. (a) Evolution of the renormalized density of states vs frequency dependence with temperature for the Einstein spectrum with $a=0.1$ and $\Omega=0.1$ ($\lambda=2$). Different curves correspond to $t=0.1, 0.05, 0.03, 0.02, 0.01, 0.0075, 0.005, 0.0025, 0.001, 0.00075, 0.0005, 0.00025, 0.0001$ from bottom to top at $\omega=0.09$. Horizontal line $N=0.05$ illustrates the band edge definition of Eq. (49). (b) Temperature dependence of ω_{edge} defined by Eq. (49) (symbols) and Eqs. (27) and (50) (heavy curves). Shown are results for $a=0.1$ and $\Omega=0.1$ (triangles, heavy solid curve) and $a=0.02$ and $\Omega=0.04$ (squares, heavy dashed curve). Thin lines simply connect the symbols.

malization of the bare band occurs that the above subdivision of the renormalized band into regions, as well as any attempt to single out characteristic features, becomes meaningless. We avoid discussing such extreme cases in this paper.

We would like to repeat and emphasize that in the present model of electron-phonon interaction, there is a definite crossover temperature which divides regimes of qualitatively different behavior of the electronic self-energy, renormalized density of states and optical quantities (see Fig. 8 below). In Sec. V we provide further discussion of t_{cros} for more general shapes of $\alpha^2F(\omega)$ and various values of parameters of the model that confirms that Eq. (48) gives the correct relation between the crossover temperature and the phonon energy scale.

Studying Fig. 7(a) one could conjecture that the renormalized band edge, ω_{edge}, can be reasonably defined in spite of the presence of high frequency tails in $N(\omega)$. This is indeed the case because $N(\omega)$ decreases quite fast at high ω. Remember that for interactions with impurities, the renormalized band edge was sharp with $N(\omega)=0$ for $\omega > \omega_{edge}$ given by Eq. (27) in that case [see also Fig. 1, where $-\Sigma_2(\omega)$ is proportional to $N(\omega)$]. In the present case of interaction with Einstein phonons $N(\omega)$ decays exponentially as $\omega \to \infty$, as shown in subsection A above [see Eq. (43)]. Therefore we choose to define the band edge ω_{edge} by a cutoff procedure using the relation

$$N(\omega_{edge}) = 0.05. \tag{49}$$

Of course, this 5% cutoff is somewhat arbitrary and using a different percentage would give slightly different results for ω_{edge}. To grasp the main dependence of ω_{edge} on temperature we note that, at high frequencies, the Einstein frequency Ω can be neglected in Eqs. (35) and (38). In this case they become identical to the self-energy equations for impurity scattering with modified interaction strength

$$\gamma_{eff}(t) = a(2n(\Omega) + 1) = a/\tanh(\Omega/2t). \tag{50}$$

To evaluate the band edge position we now can use Eq. (27) obtained previously in Sec. III. In Fig. 7(b) we show the temperature variation of ω_{edge} found using the definition of Eq. (49) along with the dependence given by Eqs. (27) and (50) for $a=0.1$, $\Omega=0.1$ (triangles, solid curve) and $a=0.02$, $\Omega=0.04$ (squares, dashed curve). Both definitions give very similar qualitative temperature dependence for the renormalized band edge. The absolute values of ω_{edge} from the two definitions differ the most at low temperatures, by about 6% and 4%, respectively, for the above sets of parameters, and become closer to each other at higher t.

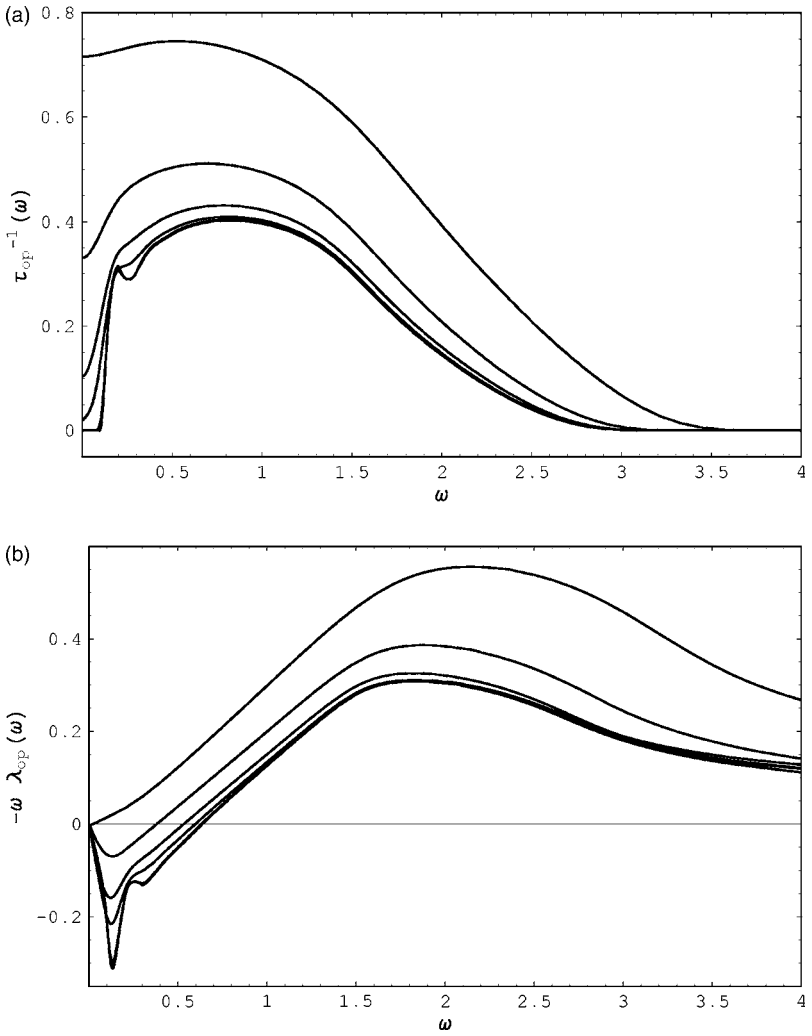

FIG. 8. Evolution of the memory function vs frequency dependence with temperature for the Einstein spectrum with $a=0.1$ and $\Omega=0.1$ ($\lambda=2$). Frame (a) is for the real part, $\tau_{op}^{-1}(\omega)$, while frame (b) is for the imaginary part, $-\omega\lambda_{op}(\omega)$. In each frame different curves correspond to $t=0.1,0.05,0.03,0.02,0.005,0.0025,0.001$ from top to bottom at $\omega=0.09$ in frame (a) and at $\omega=0.9$ in frame (b).

Finally, for completeness, the temperature dependence of the optical characteristics, $\tau_{op}^{-1}(\omega)$ [frame (a)] and $-\omega\lambda_{op}(\omega)$ [frame (b)], is presented in Fig. 8. Here we used the same parameters $a=0.1$, $\Omega=0.1$ as for the self-energies in Fig. 6. Temperatures used are $t=0.001,0.0025,0.005,0.02,0.03,0.05,0.1$. Note the filling of the low energy gap in $\tau_{op}^{-1}(\omega)$ at $t\gtrsim 0.02$ analogous to the situation for $\Sigma_2(\omega)$ discussed above. Also as t increases the low frequency negative peak in $-\omega\lambda_{op}(\omega)$ of Fig. 8(b) is gradually reduced and disappears completely at the highest temperature shown.

C. Other models for electronic dispersion and generic features due to finite bandwidth

Before we proceed to discuss more general forms of the electron-phonon spectral function $\alpha^2F(\omega)$ let us make a digression and consider some other choices for the electron dispersion.

1. Electron group velocity model for tight binding dispersion in 2D

In all calculations of the optical conductivity up to this point we have assumed that the averaged square of the group velocity, Eq. (6), is defined by the free electron dispersion [see Eq. (7)]. Here we consider another model for V_ξ^2 in order to see what type of change might arise. In the general formulas for $\sigma_1(\omega)$ in Eq. (16), we insert the expression

$$V_\xi^2=\frac{W}{D}\frac{\hbar^2}{2m_b}\left[1-\left(\frac{\xi}{W/2}\right)^2\right], \tag{51}$$

which is appropriate for an approximate treatment of a nearest neighbor tight binding band in two spatial dimensions.[50] In this equation m_b is the band mass of electron. Note that now to make the optical conductivity dimensionless we normalize it by $\pi e^2/[4Dm_b(W/2)]$, as opposed to $\pi e^2/[2Dm(W/2)]$ used in the case of quadratic dispersion. The results for $\tau_{op}^{-1}(\omega)$ and $-\omega\lambda_{op}(\omega)$ are presented in Fig. 9(a) for $a=0.1$, $\Omega=0.1$ and $t=0.0001$ by heavy lines, solid and dashed, respectively. Previous results for these quantities with the same parameters for quadratic dispersion are also shown by thin lines for comparison. We see no qualitative difference between these two sets of curves. Only small quantitative changes are found. Note, in particular, that the phonon structure at low ω is pretty well unaltered.

2. Semielliptic bare DOS model

Our model for the bare band DOS, Eq. (2), may seem somewhat unrealistic in that it has a sharp band edge, where

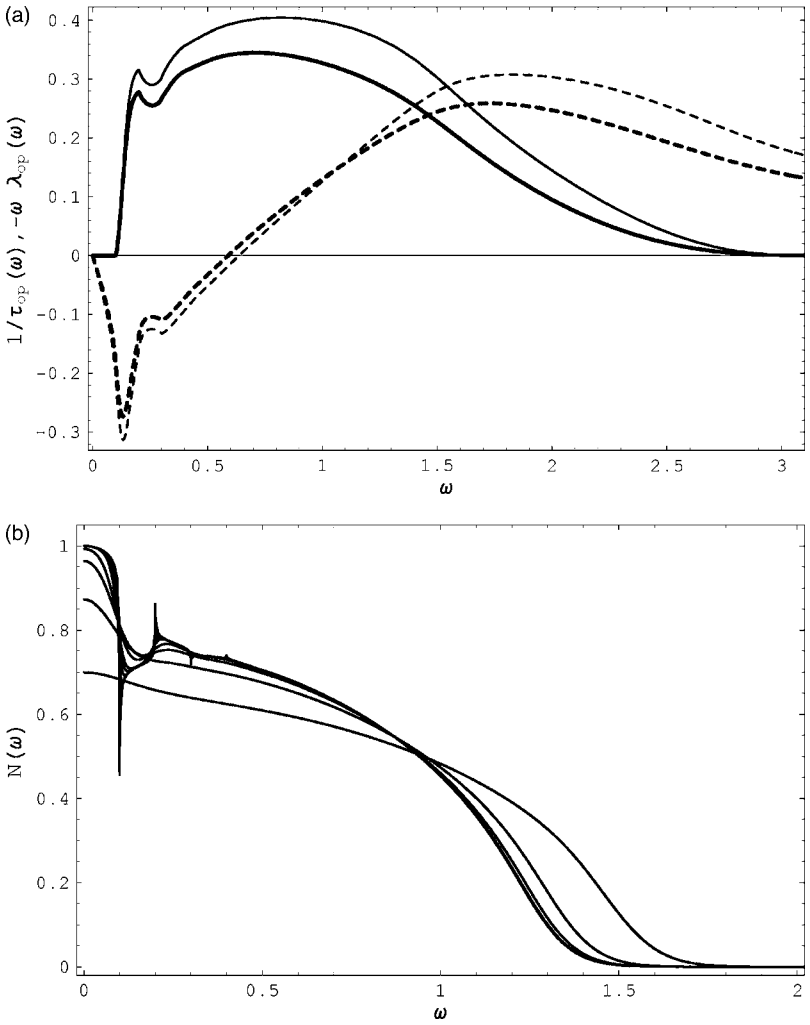

FIG. 9. (a) Comparison of optical quantities for quadratic (thin curves) and tight binding (heavy curves) models of the electronic dispersion with sharp bare band edges. Solid curves are for scattering rate $\tau_{op}^{-1}(\omega)$ while dashed curves are for $-\omega\lambda_{op}(\omega)$. (b) Evolution of the renormalized density of states vs frequency dependence with temperature for semielliptic bare band of Eq. (52). This should be compared with Fig. 7(a). Different curves correspond to $t=0.1, 0.05, 0.03, 0.02, 0.01, 0.0075, 0.005, 0.0025, 0.001, 0.00075, 0.0005, 0.00025, 0.0001$ from bottom to top at $\omega=0.09$. The $\alpha^2F(\omega)$ used in both frames is the Einstein mode with $a=0.1$ and $\Omega=0.1$ ($\lambda=2$).

$N_0(\xi)$ drops discontinuously. This is a reasonable choice for compounds whose electronic system is effectively 2D,[50] but for a 3D electronic system the nature of the van Hove singularity at the band edge is different; $N_0(\xi)$ vanishes continuously, but $dN_0(\xi)/d\xi$ is infinite. Therefore, we now switch to the semielliptic bare DOS,

$$N_0(\xi) = N_0\sqrt{1-\left(\frac{\xi}{W/2}\right)^2}, \tag{52}$$

in order to understand to what extent the finite bandwidth features of the spectroscopic characteristics that we discussed in the previous two sections are the consequences of the sharp band edge assumption. To maintain the total number of states in the band equal to 1, as in Eq. (2) we choose $N_0=4/(\pi W)$ and this value is used as the unit for both bare and renormalized density of states below, until the end of this subsection. The energy unit $W/2$ does not change. Using Eq. (52) to calculate the $\eta(z)$ function of Eq. (11) we obtain

$$\eta(z) = \pi u(z)[1-\sqrt{1-1/u(z)^2}], \tag{53}$$

where $u(z)=z-\Sigma(z)$. On the imaginary axis, this becomes

$$\eta_{im}(i\omega_n) = \pi i(\omega_n + i\Sigma_{im}(i\omega_n)) \times\left[1+\sqrt{1-\frac{1}{(\omega_n+i\Sigma_{im}(i\omega_n))^2}}\right], \tag{54}$$

where both $\Sigma_{im}(i\omega_n)$ and $\eta_{im}(i\omega_n)$ are pure imaginary. Just above the real axis, Eq. (53) applies with $z\to\omega+i\delta$ and the principal branch is taken in the square root ($\mathrm{Re}(\sqrt{\ldots})>0$). Using ω as a shorthand for $\omega+i0^+$, we obtain

$$\eta_1(\omega) = \pi[\omega-\Sigma_1(\omega)-R_+(\omega)R_-(\omega)\cos\phi(\omega)], \tag{55}$$

$$\eta_2(\omega) = -\pi[\Sigma_2(\omega)+R_+(\omega)R_-(\omega)\sin\phi(\omega)], \tag{56}$$

$$R_\pm(\omega) = \sqrt[4]{[\omega-\Sigma_1(\omega)\pm 1]^2+[\Sigma_2(\omega)]^2}, \tag{57}$$

$$\phi(\omega) = \frac{1}{2}\left[\tan^{-1}\frac{-\Sigma_2(\omega)}{\omega-\Sigma_1(\omega)-1}+\tan^{-1}\frac{-\Sigma_2(\omega)}{\omega-\Sigma_1(\omega)+1}\right] + \frac{\pi}{2}[\Theta(\Sigma_1(\omega)-\omega+1)+\Theta(\Sigma_1(\omega)-\omega-1)]. \tag{58}$$

The results for the renormalized density of states based on the bare DOS of Eq. (52) are shown in Fig. 9(b) for $a=0.1$, $\Omega=0.1$ and for various temperatures. Comparing this figure

with Fig. 7(a), where the renormalized density of state is presented for the same parameters but for the sharp cutoff bare DOS of Eq. (2), we see that our main conclusion about the effect of the finite bandwidth on the quasiparticles DOS is not changed qualitatively. In Fig. 9(b) there is still a low energy plateau structure of enhanced DOS, and there is a strong band broadening and density of states redistribution starting above the same crossover temperature $t_{cros}=0.01$ as that for Fig. 7(a).

V. PHONON SCATTERING: PHONON ENERGY SCALE AND ELECTRON-PHONON INTERACTION STRENGTH DEPENDENCIES

In the previous section we discussed in detail finite bandwidth effects within the single Einstein mode model for the electron-phonon interaction and for a representative set of parameters: $\Omega=0.1$ and $a=0.1$ corresponding to $\lambda=2$. In this section we want to sweep the parameter space in order to see where and when those effects are the biggest.

We also include in our considerations more general forms of the Eliashberg function $\alpha^2F(\omega)$. Both mass enhancement parameter λ and the interaction strength a are given in terms of integrals involving the Eliashberg function as follows:

$$\lambda = 2\int_0^\infty \omega^{-1}\alpha^2F(\omega)d\omega, \tag{59}$$

$$a = \int_0^\infty \alpha^2F(\omega)d\omega. \tag{60}$$

Additionally, a convenient parameter to quantify the phonon energy scale, which is routinely used in the literature, is the logarithmic frequency[51] defined by

$$\omega_{\ln} \equiv \exp\left[\frac{2}{\lambda}\int_0^\infty \omega^{-1}\ln(\omega)\alpha^2F(\omega)d\omega\right]. \tag{61}$$

Naturally, for an Einstein model $\omega_{\ln}=\Omega$. To discuss the electron phonon interactions in the present section we use $\omega_{\ln}$, λ and a parameters. Remember, that λ is dimensionless according to its definition, Eq. (59). Both $\omega_{\ln}$ and a have the dimension of energy and are normalized to $W/2$, half the bare bandwidth, in the units we use.

One model of $\alpha^2F(\omega)$ we used is a truncated Lorentzian centered at $\omega=\Omega$:

$$\alpha^2F(\omega) = \frac{R(\lambda)}{2\pi}\left[\frac{\delta}{(\omega-\Omega)^2+\delta^2} - \frac{\delta}{\eta^2+\delta^2}\right]\Theta(\eta-|\omega-\Omega|), \tag{62}$$

where parameter δ controls the half-width of the peak and the full width of $\alpha^2F(\omega)$ is equal to 2η. The rescaling factor $R(\lambda)$ is inserted to guarantee a chosen value of λ. Such spectrum is often used in the literature to introduce a smearing of the simple Einstein mode spectrum.[3,17] For our numerical work we used $\delta=0.06\Omega$ and $\eta=\Omega/4$, while the value of Ω was varied. To compare with the results for the Einstein model in previous sections we used $\lambda=2$.

Another model of $\alpha^2F(\omega)$ that we employed to simulate a distributed spectrum is a three frequency model:

$$\alpha^2F(\omega) = \lambda\sum_{i=1}^{3}\frac{\omega_i l_i}{2}\delta(\omega-\omega_i), \tag{63}$$

with $\Sigma_{i=1}^3 l_1=1$. Motivated by the electron-phonon interaction in the fulleride compound K_3C_{60} we set $\lambda=0.71$ with $l_1=0.3$, $l_2=0.2$, $l_3=0.5$ and $\omega_1:\omega_2:\omega_3=0.04:0.09:0.19$.[16] Then the value of $\omega_{\ln}$ was varied.

First we consider the crossover temperature t_{cros} introduced in Eq. (48) by considering the case of Einstein electron-phonon spectral function with $a=0.1$ and $\Omega=0.1$. Now we use a more general truncated Lorentzian model of $\alpha^2F(\omega)$ with various values of $\omega_{\ln}$ and a. As mentioned earlier, t_{cros} can be defined using various features of the self-energy $\Sigma(\omega)$, both at low and high energies. We choose to analyze the quantity $-d\Sigma_1(\omega=0)/d\omega$, for which an analytic expression is available in the case of an infinite band (see for example Ref. 52). For the Einstein model, with $\Omega=\omega_{\ln}$ and $a=\lambda\omega_{\ln}/2$, it has a simple form:

$$-\frac{d\Sigma_1(0)}{d\omega} = -\frac{\lambda}{\tau}\,\mathrm{Im}\,\psi'\left(\frac{1}{2}+\frac{i}{\tau}\right), \quad \tau = 2\pi\frac{t}{\omega_{\ln}} \tag{64}$$

where $\psi(z)$ is the logarithmic derivative of the gamma function. In Fig. 10 we show the numerically calculated $\Sigma_1'(0)$ for $\omega_{\ln}=0.1$ (diamonds), 0.01 (squares), and 0.001 (triangles) with $a=0.1$, 0.01 and 0.001, respectively, all corresponding to $\lambda\approx 2$. Thin lines are given to guide the eyes. Note the logarithmic scale on the horizontal axis, which is required to make our low temperature data more clearly visible. We observe that there is a noticeable dependence on a in the three sets of data presented. In particular, the limiting value of $-\Sigma_1'(0)$ as $t\to 0$ and the temperature at which $\Sigma_1'(0)=0$ depends on a quite strongly. However, the position of maxima in the $-\Sigma_1'(0)$ vs t dependence is almost the same, for all three a values. It is also very close to $t_{\max}\simeq 0.485\omega_{\ln}$ which is the position of the maximum in the heavy solid curve corresponding to Eq. (64). According to this equation the ratio $t_{\max}/\omega_{\ln}$ is a universal number, i.e., it is not influenced by a or λ. It is then useful to define the crossover temperature t_{cros} relative to $t_{\max}$. For all the above sets of parameters for the electron-phonon interaction we have performed an analysis of the self-energy data, similar to those presented in Figs. 6 and 7. Our conclusion is that t_{cros} can be approximately associated with temperature where the curves $-\Sigma_1'(0)$ vs $\ln(t/\omega_{\ln})$ start to increase significantly after being flat at low t, which corresponds $\ln(t_{cros}/\omega_{\ln})\approx -2.25$ or

$$t_{cros} = 0.1\omega_{\ln}. \tag{65}$$

These considerations extend our previous particular result, Eq. (48). We conclude that the crossover temperature depends mostly on the phonon energy scale, and not on the characteristics of the interaction.

Next, we turn to consider the two important effects of a finite bandwidth in the renormalized density of states described in the previous section: the magnitude $\delta N_{plateau}$ of the elevated plateau feature at low energies, $\omega\lesssim\omega_{\ln}$, which is

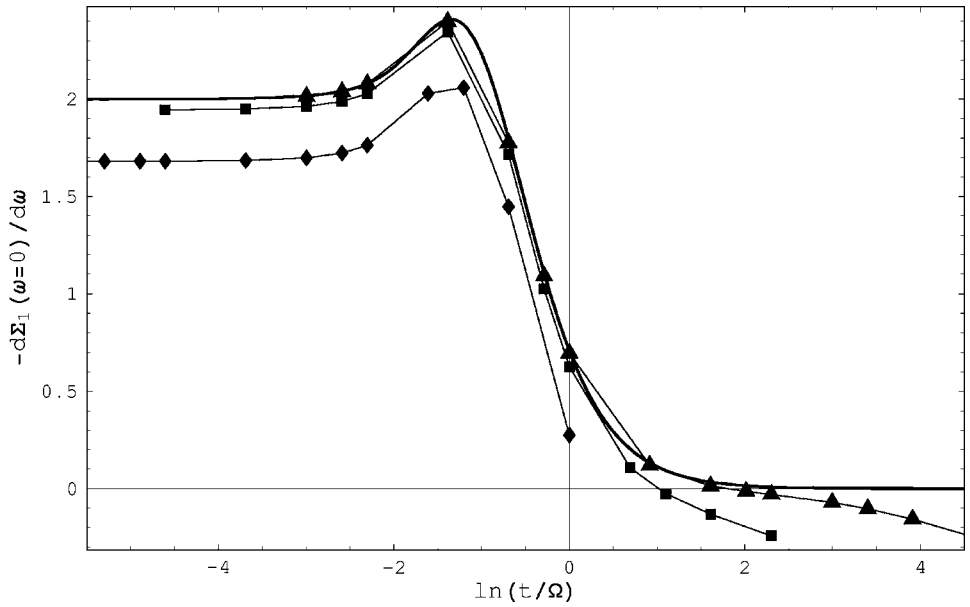

FIG. 10. The temperature dependence of the minus first derivative of the real part of the self-energy at the Fermi level, namely $-d\Sigma_1(\omega=0)/d\omega$. All numerical results are for the truncated Lorentzian $\alpha^2F(\omega)$ of Eq. (62) with $\omega_{\ln}=0.1$ (diamonds), 0.01 (squares), and 0.001 (triangles). The heavy solid curve shows the infinite band result of Eq. (64); thin solid lines simply join numerical points.

best defined at $t \lesssim t_{cros}$, and a temperature driven increase of the renormalized band edge, which starts to occur at $t \gtrsim t_{cros}$. We use various models for $\alpha^2F(\omega)$ and find that both effects depend mostly on the interaction strength a, Eq. (60), while they are much less sensitive to the mass enhancement parameter λ, Eq. (59).

In Fig. 11(a) we show $N(\omega)$ vs $\omega/\omega_{\ln}$ in the low frequency region. Dashed curves are results for the Einstein model of $\alpha^2F(\omega)$ with $(a,\lambda)=(0.001,2)$, (0.01,2), and (0.1,2) (from top to the bottom), solid curves are for the truncated Lorentzian $\alpha^2F(\omega)$ with $(a,\lambda)=(0.02,1)$, (0.05,1), and (0.1,2) (from top to the bottom), while dotted curves are for the three frequency model of $\alpha^2F(\omega)$ with $(a,\lambda)=(0.018,0.71)$ and (0.036,0.71) (from top to the bottom). All the results shown are for a finite temperature, a little different in units of $\omega_{\ln}$ in different cases, but always well below t_{cros} of Eq. (65).

We define the magnitude of the elevated plateau feature by the relation

$$\delta N_{plateau} \equiv N(0) - N(4\omega_{\ln}). \tag{66}$$

The value $4\omega_{\ln}$ was chosen such that almost all of the curves presented in Fig. 11(a) are flat in the region $\omega \approx 4\omega_{\ln}$. The multiphonon features clearly visible at lower energies are damped sufficiently strongly this far from the Fermi level so that the DOS is nearly flat except for the lowest three curves in Fig. 11(a). These correspond to rather large values of $\omega_{\ln}$ in the units of the half bandwidth, $W/2$. In this situation the definition of the finite band effects we have discussed starts to become less sharp. Nevertheless, it is possible to pick the value of $4\omega_{\ln}$ for the purpose of our argument.

The magnitude of the plateau determined from Fig. 11(a) is plotted vs the strength of the interaction a in Fig. 11(b). Squares are for the Einstein model of $\alpha^2F(\omega)$, triangles are for the truncated Lorentzian, and diamonds are for the three frequency model. All the data, except those for the largest $a=0.1$, fall very close on the straight line $\delta N_{plateau}(a)=2a$ which is also shown in the figure. On the other hand, we observe no dependence on λ.

The two lowest curves in Fig. 11(a), which are nearly overlapping, correspond to the same parameters $a=0.1$ and $\lambda=2$, but with different choice of $\alpha^2F(\omega)$: the sharper curve is for the Einstein model while the more rounded curve is for the truncated Lorentzian model. The shape of $\alpha^2F(\omega)$, thus, is not essential for the analysis of the overall behavior of $N(\omega)$ and for $\delta N_{plateau}$ in particular. The other thing to notice is that the infinite band result for $N(\omega)$, which is completely flat, is gradually recovered as $\omega_{\ln}$ decreases. The top solid curve in Fig. 11(a) corresponds to $\omega_{\ln}=0.001$ and no features can be distinguished on scale of the figure, although they are actually present and, in particular, $\delta N_{plateau}=0.2\%$ in this case.

The renormalized band edge is another quantity that depends on the parameters specifying the electron-phonon interaction. The consideration of the Einstein spectrum in Sec. IV has shown that at high temperatures ω_{edge} behaves according to Eq. (50) while at low t it is almost temperature independent [see Fig. 7(b)]. Here we perform an analysis of the renormalized band edge at $t=0$ using the definition given in Eq. (49). For the case of ω_{edge}, as opposed to the previously studied case of $\delta N_{plateau}$, we do not expect the quality of its numerical definition to deteriorate as a increases. The results for ω_{edge} vs a at $t=0$ are plotted in Fig. 11(c) for the same $\alpha^2F(\omega)$ model and parameters used in Figs. 11(a) and 11(b). We again tried to fit the data with a single analytical dependence and found that the relation $\omega_{edge}(a)=1+2.5a^{0.68}$ works reasonably well. The deviation of the symbols from the solid curve in Fig. 1(c) can be attributed to some λ dependence, which is weak but apparently present in the case of ω_{edge}.

To conclude this section, in Fig. 12 we return to the features induced by a finite bandwidth in the optical characteristics of Eqs. (20) and (21). Dotted curves are for the Einstein model of $\alpha^2F(\omega)$ with $a=0.1$ while dashed curves are for the truncated Lorentzian model of $\alpha^2F(\omega)$ with $a=0.01$.

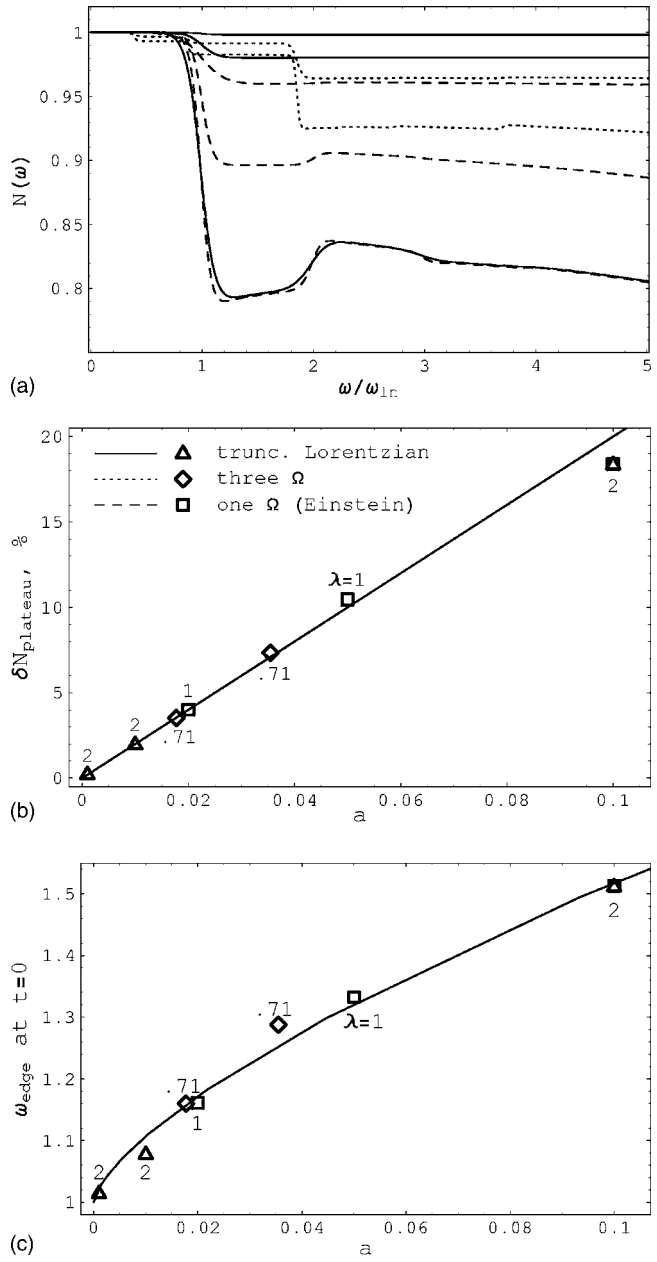

FIG. 11. (a) Frequency dependence of the renormalized density of states $N(\omega)$ in the region of phonon frequencies for a variety of $\alpha^2F(\omega)$ models, which are specified in frame (b). See text for a complete explanation. (b) Relative height of the plateau feature in $N(\omega)$ at $\omega \lesssim \omega_{\ln}$ as a function of the coupling strength a for a variety of $\alpha^2F(\omega)$ models (symbols). Line shows the best polynomial fit $\delta N_{plateau}(a)=2a$. (c) Dependence of ω_{edge} defined by Eq. (49) on the coupling strength a for the same models (symbols). Line shows the best polynomial fit $\omega_{edge}(a)=1+2.5a^{0.68}$.

In both cases $\lambda=2$ and $t/\omega_{\ln}=0.001$, i.e., practically zero. For comparison we also present the infinite band results (solid curves) for an Einstein model with $a=0.1$ at zero temperature [see Eqs. (47) and (46)]. The scale of the overall magnitude of both the optical scattering rate $\tau_{op}^{-1}(\omega)$ in Fig. 12(a) and the optical mass renormalization $-\omega\lambda_{op}(\omega)$ in Fig. 12(b) is given by a. All the results are scaled by $2\pi a$ so that the infinite band curves would approach 1 as $\omega \to \infty$. Note that this scale is a consequence of the presence of the electron-phonon interaction itself rather than the presence of a finite band. The finite band effects manifest themselves in the deviations of dashed and dotted curves from the solid one; these deviations are much bigger for the dotted curve. This demonstrates that our conclusions about a strong dependence of finite band effects on the a parameter hold true for the optical characteristics. It also shows that the additional boson structures, seen very clearly in the dotted curve at $\omega=2\Omega$ and 3Ω and hardly seen in the long dashed curve, are completely absent from the solid curve which is smooth. The Einstein boson manifests itself in this curve, corresponding to the infinite band, only in its rise out of zero at $\omega=\Omega$.

This rise is slightly modified in the dotted curve and smeared slightly below $\omega=\Omega$ in the long dashed curve because of the extended Lorentzian spectrum that was used instead of the delta function.

VI. APPLYING INFINITE BAND FORMULAS TO ANALYSIS OF THE FINITE BAND RESULTS

We have seen that as Ω or $\omega_{\ln}$ decreases relative to the bare bandwidth (note that our unit of energy is $W/2$, so that Ω has to be compared to the energy scale of unity) finite band effects become less prominent, even though they are not washed out completely. In the case $\Omega \ll 1$ the various formulas derived for the infinite band should become applicable. In this section we consider two examples in order to gain an understanding of the limitations of analysis based on these "standard" expressions.

A. The large ω region for $\sigma_1(\omega)$

Recently, Karakozov, Maksimov, and Dolgov[53] have considered the large ω limit of the optical conductivity $\sigma_1(\omega)$ for an infinite band. For $\omega \gg \{\omega_{\ln}, \Gamma_{ph}\}$, where Γ_{ph} is a measure of damping due to phonons, they derived

$$\sigma_1(\omega) \approx \frac{\omega_{pl}^2}{4\pi} \frac{\Gamma_{asympt}(T)}{\omega^2}, \tag{67}$$

where the scattering rate

$$\Gamma_{asympt}(T) = 2\pi \int_0^\infty d\nu\, \alpha^2F(\nu) \coth \frac{\nu}{2T} \tag{68}$$

depends only on temperature. For a finite band such a relationship can no longer hold at large ω where the finite band nature of the problem profoundly changes the frequency and temperature dependence of $\sigma_1(\omega,T)$ as we have seen. Nevertheless, it is of considerable interest to consider when Ω is small (i.e., small phonon energy as compared to half bandwidth) but still finite, if there exists some ω regime where Eqs. (67) and (68) still hold approximately. That such a regime does indeed remain is illustrated in the inset of Fig. 13. For the figure we have used $a=0.001$ and $\Omega=0.001$ and the solid curve in the inset is for $t/\Omega=0.05$, i.e., low temperature as compared with Ω. We plot the quantity $\omega^2\sigma_1(\omega)$, normalized by its maximum value, as a function of ω which is seen to rise rapidly towards a value 1 in our normalization, and

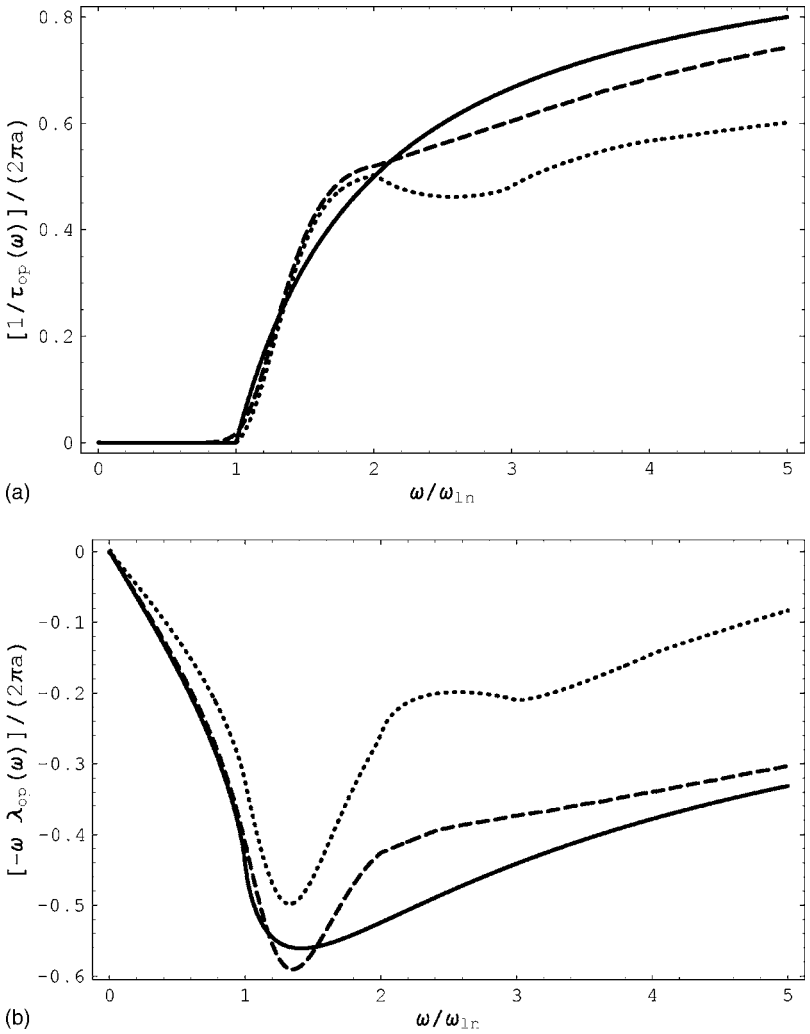

FIG. 12. Frequency dependence of the memory function normalized by $2\pi a$. Frame (a) is for the real part, $\tau_{op}^{-1}(\omega)$, while frame (b) is for the minus imaginary part, $-\omega\lambda_{op}(\omega)$. Dashed curves are for the truncated Lorentzian $\alpha^2F(\omega)$ with $\omega_{\ln}=0.01$ while dotted curves are for the Einstein mode $\alpha^2F(\omega)$ with $\Omega=0.1$. Temperature $t=0.0001$ in both cases. Solid curves give the infinite band results at $t=0$ for comparison.

retains this same value from $\omega\approx 0.1$ up to the renormalized band edge. At this point it drops quite sharply and, in this large ω region, $\sigma_1(\omega)$ becomes small much faster than the ω^{-2} law of the Drude model. The dashed curve is for a model with larger $\Omega=0.01$ and $a=0.01$. Now the frequency region where $\sigma_1(\omega)$ obeys a ω^{-2} law is greatly reduced but it is still identifiable. In the main frame of Fig. 13 we show results obtained for the constant $\Gamma(t)$ vs t in the flat region of

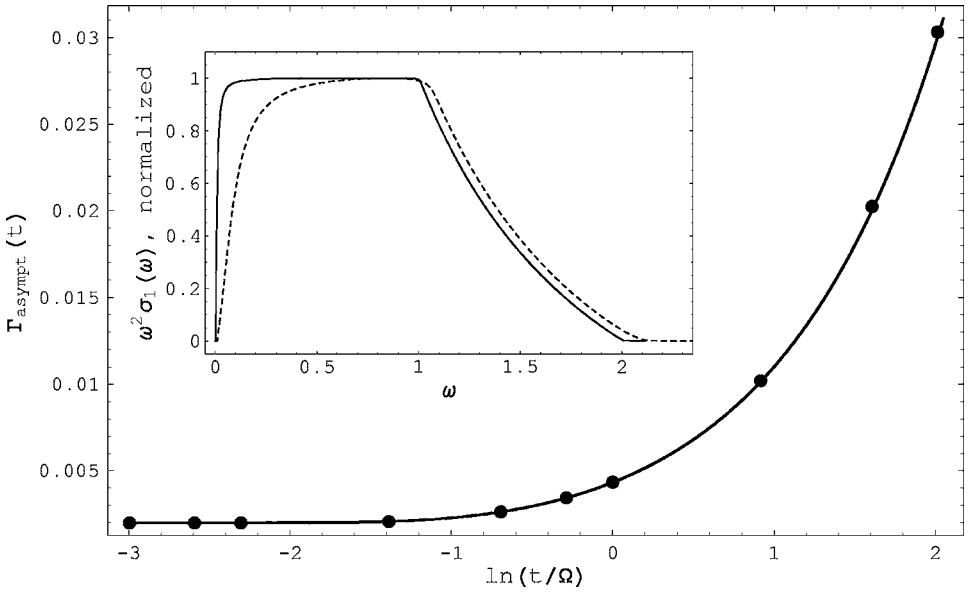

FIG. 13. The region of Drude behavior for optical conductivity in a finite band can be defined as $\omega^2\sigma_1(\omega)\approx$ const which is demonstrated in the inset for $a=0.001, \Omega=0.001$ (solid curve) and $a=0.01, \Omega=0.01$ (dashed curve), with temperature set to 0.05Ω in each case. The main frame shows our numerical results for the temperature dependence of the scattering rate defined by Eq. (67) in this region (solid circles) along with the infinite band results of Eq. (68) (solid curve).

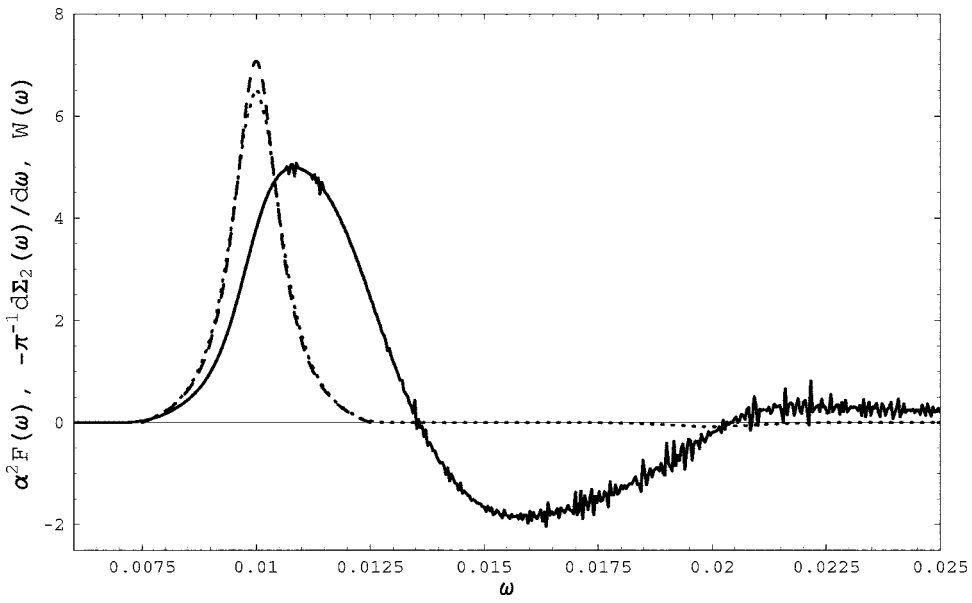

FIG. 14. The frequency dependences of the inversion function $W(\omega)$ of Eq. (69) (solid curve) and of $-\pi^{-1}d\Sigma_2(\omega)/d\omega$(dotted curve) obtained in our numerical calculations. The input $\alpha^2F(\omega)$ (dashed curve) is the truncated Lorentzian of Eq. (62) centered at $\omega=0.01$.

$\omega^2\sigma_1(\omega,t)$ for $a=0.001$ and $\Omega=0.001$. The solid circles are the results of our calculations while the continuous curve was obtained from Eq. (68). This curve agrees very well with the solid circles. Thus we are able to identify a range for which Eq. (67) holds with $\Gamma(t)$ given by Eq. (68) but the frequency regime over which this holds becomes small for $\Omega=0.01$ (see dashed curve in the inset of Fig. 13). At higher frequencies, finite band effects dominate the conductivity and concepts based on an infinite band cease to be valid.

B. The "double derivative" formula for $\alpha^2F(\omega)$

Perhaps a more stringent test of the approach of our finite band results, to the infinite band case as Ω is reduced, is provided in Fig. 14. In a previous paper, Marsiglio, Startseva, and Carbotte[54] have shown, through numerical calculations of the optical conductivity for the electron-phonon spectral density $\alpha^2F(\omega)$ of Pb, that the function

$$W(\omega)=\frac{1}{2\pi}\frac{d^2}{d\omega^2}[\omega\tau_{op}^{-1}(\omega)], \tag{69}$$

with $\tau_{op}^{-1}(\omega)$ given by Eq. (20) in the infinite band case at zero temperature, has a profile very reminiscent to the profile of the input $\alpha^2F(\omega)$, provided that negative tails present in $W(\omega)$ beyond the cutoff in $\alpha^2F(\omega)$ are ignored. Not only does $W(\omega)$ have the same shape as $\alpha^2F(\omega)$, but it has nearly the same area, which is a dimensionless measure of the interaction strength. Below we want to check if this "inversion" procedure remains effective in the finite band case.

In Fig. 14 we show the second derivative of $\omega\tau_{op}^{-1}(\omega)$ (solid curve) which defines $W(\omega)$. (The curve is not smooth at higher ω due to our numerical second derivative.) This result was obtained with an $\alpha^2F(\omega)$ given as the truncated Lorentzian centered at $\Omega=0.01$, which is also shown for comparison as the dashed curve. We see that $W(\omega)$ is broader than the input $\alpha^2F(\omega)$ and shifted to higher energies. More importantly, the area under the first peak in $W(\omega)$, up to the frequency where it first becomes negative, is about 46% larger than that under $\alpha^2F(\omega)$. However, this effect is not due to finite bandwidth, but rather the consequence of the particular form of the input $\alpha^2F(\omega)$ we used here. It turns out that the inversion procedure of Eq. (69) becomes less accurate for a relatively narrow peaked spectrum, while it is quite precise for an extended broad spectrum as was found in Ref. 54. The finite band effects, appearing on top of the spectrum shape effects, are small. We found that for $\Omega=0.01$ the area under $W(\omega)$ is smaller than its infinite band value by just 2%.

On the other hand, the dotted curve, which was obtained from a first derivative of $\Sigma_2(\omega)$ over ω, i.e., from the corresponding quasiparticle scattering rate, overlaps almost perfectly with the input $\alpha^2F(\omega)$ (dashed). In this instance the spectrum shape effects are absent and to a good approximation we recover the known infinite band results that $\alpha^2F(\omega)=-\pi^{-1}d\Sigma_2(\omega)/d\omega$ at $t=0$. The finite band effects here are negligible.

Recently, there have been a number of attempts to "invert" spectroscopic experimental data on high-T_c cuprates in order to extract the underlying electron-boson spectral function.[49,55–57] They include both simpler approaches based on derivative formulas like Eq. (69) and more sophisticated ones that deal with integral equations. We want to comment that if the electron-phonon spectral density $\alpha^2F(\omega)$ has a narrow peak then inversion of photoemission data should produce accurate results while inversion of optical data could possibly be hindered by shifts in positions of peaks in $\alpha^2F(\omega)$ and an overestimate of the overall coupling strength.

VII. CONCLUSIONS

Much of the literature on the effect of impurities or coupling to phonons in metals has assumed infinite electronic bands. This assumption is believed to be appropriate if one is interested in properties that probe mainly what happens to electrons near the Fermi surface on an energy scale much less than the bandwidth W. Here we considered the effects of a finite bare band on renormalization due to interactions with

impurities as well as with phonons. Free electrons as well as tight binding bands are employed in an approximation where a sharp cutoff is applied on the bare band density of states at $\pm W/2$ with constant density in between. A semielliptic bare DOS is also considered but no qualitative differences are found.

The interaction of electrons with impurities or with phonons through the electron-phonon coupling changes their self energy and leads to quasiparticle mass renormalization and damping. The band edge is also modified, becoming rounded and smeared by the interactions. Spectral weight is shifted from low energies to energies above the bare band edge ($W/2$). For coupling to impurities a sharp cutoff persists for the renormalized bands. For coupling to phonons a cutoff can still be defined although it is not strictly sharp as small tails extend exponentially to high energies. The width of the renormalized bands increases with increasing strength of the coupling to both impurities and phonons as well as with increasing temperature (for phonons). For impurity scattering the real part of the electron self-energy is always positive exhibiting a characteristic sharp peak at the renormalized band edge before dropping rapidly at first and then more slowly (with upward curvature). It remains significant in value even at four times the bare half bandwidth. This is to be contrasted with the infinite bandwidth case for which the real part of the self-energy is zero. On the other hand, the imaginary part, which is proportional to the renormalized density of states $N(\omega)$, drops precipitously at the renormalized band edge. In the infinite bandwidth case it would be constant for any value of ω however large.

Optical properties were computed and compared with the self-energy. The optical mass renormalization, $-\omega\lambda_{op}(\omega)$, was found to follow the behavior of $\Sigma_1(\omega)$ with several differences. At $\omega \to 0$ both are linear in ω but the optical quantity is larger. At the bare band edge there are no sharp peaks in $-\omega\lambda_{op}(\omega)$. Rather there is a much broader peak centered at somewhat higher energy. In this region (high ω) it remains considerably above $\Sigma_1(\omega)$. There is also optical spectral weight redistribution in the real part of the conductivity $\sigma_1(\omega)$. The dc conductivity is enhanced and at high frequencies, $\sigma_1(\omega)$ falls below its infinite band Drude form.

For phonons several models were considered for the electron-phonon spectral density, $\alpha^2F(\omega)$, including the Einstein oscillator, the three frequency model of Eq. (63), as well as the truncated Lorentzian model of Eq. (62). An important characteristic of the low energy renormalized density of states $N(\omega)$ is that, while constant and equal to its bare value up to ω_E for the Einstein case, beyond this energy it shows a drop as well as additional phonon induced structures. These structures are not present in the infinite band. Their amplitude is approximately proportional to the area under the $\alpha^2F(\omega)$ curve, denoted by a in this paper. The missing low energy spectral weight is transferred to higher energies much as in the impurity case. The band broadens and the sharp cutoff of the bare band becomes smeared. However, a renormalized band edge is still definable. The plateau structure in $N(\omega)$ at low energy, due entirely to the finite band cutoff, is reflected in the imaginary part of Σ and also in the optical scattering rate. This boson structure smears out as temperature is increased and additional spectral weight is transferred to higher energies. Beyond the renormalized band edge, the optical scattering rate drops but remains finite until approximately twice this frequency where it is still not zero but becomes negligible. In contrast to the infinite band, where the real part of the self-energy, $\Sigma_1(\omega)$ [or $-\omega\lambda_{op}(\omega)$], is negative for all frequencies, for a finite band they both go through zero on the scale of the phonon energy involved, and become positive followed by a slow decay with increasing ω. The low energy structure is sharper and narrower for $\Sigma_1(\omega)$ than it is for $-\omega\lambda_{op}(\omega)$. This low energy negative renormalization is progressively reduced with increasing temperatures. At high temperatures both $\Sigma_1(\omega)$ and $-\omega\lambda_{op}(\omega)$ begin to behave qualitatively like in the impurity case indicating that the thermally induced real displacements of the atoms off equilibrium simulate impurity scattering.

For very small values of the phonon energy scale relative to the bandwidth, denoted by $\omega_{\ln}$, we find a regime where $\sigma_1(\omega)$ shows the expected infinite band asymptotic behavior, i.e., it decreases as $1/\omega^2$ with the proportionality constant equal to the frequency independent scattering rate $\Gamma(T)$, which also takes on its infinite band temperature dependence. At still higher energies this correspondence ceases to exist and the finite band cutoff dominates the behavior of the real part of the conductivity where $\sigma_1(\omega)$ begins to drop towards zero much faster than for the Drude from.

In the process of inverting optical data in a finite band we have discovered a new regime which was not covered in Ref. 54. In their infinite band work Marsiglio, Startseva, and Carbotte[54] found a close correspondence between the function $W(\omega)$ of Eq. (69) and the underlying $\alpha^2F(\omega)$ in the phonon region of ω. In particular, both functions, which are dimensionless, have peaks at the same frequencies and the area under both curves is approximately the same. However, this expectation needs to be modified when the spectrum is peaked and not wide. The peak in $\alpha^2F(\omega)$ is shifted to somewhat higher energies in $W(\omega)$ and becomes broader, and also the area under $W(\omega)$ is now larger than the area under $\alpha^2F(\omega)$. This will need to be kept in mind when considering narrow structures in the electron-phonon spectral density.

ACKNOWLEDGMENTS

We greatly appreciate illuminating discussions on the subject with Professor F. Marsiglio and his valuable comments on the manuscript. Work is supported by the Natural Science and Engineering Research Council of Canada (NSERC) and the Canadian Institute for Advanced Research (CIAR).

[1] C. Grimaldi, E. Cappelluti, and L. Pietronero, Europhys. Lett. **42**, 667 (1998); E. Cappelluti, C. Grimaldi, and L. Pietronero, Phys. Rev. B **64**, 125104 (2001).
[2] E. Cappelluti and L. Pietronero, Phys. Rev. B **68**, 224511 (2003).
[3] F. Doğan and F. Marsiglio, Phys. Rev. B **68**, 165102 (2003).
[4] M. Calandra and O. Gunnarsson, Phys. Rev. B **66**, 205105 (2002).
[5] B. Mitrović and J. P. Carbotte, Can. J. Phys. **61**, 758 (1983); Can. J. Phys. **61**, 784 (1983).
[6] O. Gunnarsson and J. E. Han, Nature (London) **405**, 1027 (2000).
[7] S. Engelsberg and J. R. Schrieffer, Phys. Rev. **131**, 993 (1963).
[8] H. J. A. Molegraaf, C. Presura, D. van der Marel, P. H. Kes, and M. Li, Science **295**, 2239 (2002).
[9] A. F. Santander-Syro, R. P. M. S. Lobo, W. Bontemps, Z. Konstantinovic, Z. Z. Li, and H. Raffi, Europhys. Lett. **62**, 568 (2003).
[10] A. V. Boris, N. N. Kovaleva, O. V. Dolgov, T. Holden, C. T. Lin, B. Keimer, and C. Bernhard, Science **304**, 708 (2004).
[11] M. Ortolani, P. Calvani, and S. Lupi, cond-mat/0407432.
[12] A. Knigavko, J. P. Carbotte, and F. Marsiglio, Phys. Rev. B **70**, 224501 (2004).
[13] W. E. Pickett, Phys. Rev. B **26**, 1186 (1982).
[14] J. K. Freericks, A. Y. Liu, A. Quandt, and J. Geerk, Phys. Rev. B **65**, 224510 (2002).
[15] F. Marsiglio, J. Low Temp. Phys. **87**, 659 (1992).
[16] H.-Y. Choi, Phys. Rev. B **53**, 8591 (1996).
[17] J.-W. Yoo and H.-Y. Choi, Phys. Rev. B **62**, 4440 (2000).
[18] A. B. Migdal, Zh. Eksp. Teor. Fiz. **34**, 1438 (1958) [Sov. Phys. JETP **7**, 996 (1958)].
[19] P. B. Allen, Phys. Rev. B **18**, 5217 (1978).
[20] V. N. Kostur and B. Mitrovic, Phys. Rev. B **48**, 16388 (1993).
[21] O. Gunnarsson, V. Meden, and K. Schönhammer, Phys. Rev. B **50**, 10462 (1994).
[22] L. Pietronero, S. Strässler, and C. Grimaldi, Phys. Rev. B **52**, 10516 (1995).
[23] Y. Takada and T. Higuchi, Phys. Rev. B **52**, 12720 (1995).
[24] O. Gunnarsson, Rev. Mod. Phys. **69**, 575 (1997).
[25] A. Georges, G. Kotliar, W. Krauth, and M. J. Rozenberg, Rev. Mod. Phys. **68**, 13 (1996).
[26] A. J. Millis, R. Mueller, and B. I. Shraiman, Phys. Rev. B **54**, 5389 (1996).
[27] S. Ciuchi, F. de Pascule, C. Masciovecchio, and D. Feinberg, Europhys. Lett. **24**, 575 (1993).
[28] F. Marsiglio, M. Schossmann, and J. P. Carbotte, Phys. Rev. B **37**, 4965 (1988).
[29] A. Damascelli, Z. Hussain, and Z.-X. Shen, Rev. Mod. Phys. **75**, 473 (2003).
[30] F. Reinert, B. Eltner, G. Nicolay, D. Ehm, S. Schmidt, and S. Hufner, Phys. Rev. Lett. **91**, 186406 (2003).
[31] A. Chainani, T. Yokoya, T. Kiss, and S. Shin, Phys. Rev. Lett. **85**, 1966 (2000).
[32] F. Reinert, G. Nicolay, B. Eltner, D. Ehm, S. Schmidt, S. Hufner, U. Probst, and E. Bucher, Phys. Rev. Lett. **85**, 3930 (2000).
[33] T. Valla, A. V. Fedorov, P. D. Johnson, and S. L. Hulbert, Phys. Rev. Lett. **83**, 2085 (1999).
[34] M. Hengsberger, R. Fresard, D. Purdie, P. Segovia, and Y. Baer, Phys. Rev. B **60**, 10796 (1999).
[35] F. Marsiglio and J. P. Carbotte, in *The Physics of Superconductivity, Vol. I: Conventional and High T_c Superconductors*, edited by K. H. Bennemann and J. B. Ketterson (Springer-Verlag, Berlin, 2003), p. 233.
[36] S. V. Shulga, O. V. Dolgov, and E. G. Maksimov, Physica C **178**, 266 (1991).
[37] J. W. Allen and J. C. Mikkelsen, Phys. Rev. B **15**, 2952 (1977).
[38] A. V. Puchkov, D. N. Basov, and T. Timusk, J. Phys.: Condens. Matter **8**, 10049 (1996).
[39] F. Marsiglio and J. P. Carbotte, Aust. J. Phys. **50**, 975 (1997).
[40] M. A. Quijada, D. B. Tanner, R. J. Kelley, M. Onellion, H. Berger, and G. Margaritondo, Phys. Rev. B **60**, 14917 (1999).
[41] R. Kubo, J. Phys. Soc. Jpn. **12**, 570 (1957).
[42] W. Götze and P. Wölfle, Phys. Rev. B **6**, 1226 (1972).
[43] B. Arfi, Phys. Rev. B **45**, 2352 (1992).
[44] J. P. Carbotte, E. Schachinger, and J. Hwang, Phys. Rev. B **71**, 054506 (2005).
[45] A. Lanzara *et al.*, Nature (London) **412**, 510 (2001).
[46] X. J. Zhou *et al.*, Nature (London) **423**, 398 (2003).
[47] P. D. Johnson *et al.*, Phys. Rev. Lett. **87**, 177007 (2001).
[48] J. Hwang, T. Timusk, and G. D. Gu, Nature (London) **427**, 714 (2004).
[49] E. Schachinger, J. J. Tu, and J. P. Carbotte, Phys. Rev. B **67**, 214508 (2003).
[50] F. Marsiglio and J. E. Hirsch, Phys. Rev. B **41**, 6435 (1990); F. Marsiglio and J. E. Hirsch, Physica C **165**, 71 (1990).
[51] P. B. Allen and R. C. Dynes, Phys. Rev. B **12**, 905 (1975).
[52] F. Marsiglio, Phys. Rev. B **55**, 6674 (1997).
[53] A. E. Karakozov, E. G. Maksimov, and O. V. Dolgov, Solid State Commun. **124**, 119 (2002).
[54] F. Marsiglio, T. Startseva, and J. P. Carbotte, Phys. Lett. A **245**, 172 (1998).
[55] S. Verga, A. Knigavko, and F. Marsiglio, Phys. Rev. B **67**, 054503 (2003).
[56] J. Shi, S.-J. Tang, B. Wu, P. T. Sprunger, W. L. Yang, V. Brouet, X. J. Zhou, Z. Hussain, Z.-X. Shen, Z. Zhang, and E. W. Plummer, Phys. Rev. Lett. **92**, 186401 (2004).
[57] S. V. Dorcevic, C. C. Homes, J. J. Tu, T. Valla, M. Strongin, P. D. Johnson, G. D. Gu, and D. N. Basov, cond-mat/0411043.